
Article:
Hofstra, M, Hodgson, DM, Peakall, J et al. (2015) Giant scour-fills in ancient channel-lobe transition zones: Formative processes and depositional architecture. Sedimentary Geology, 329. 98 - 114. ISSN: 0037-0738

https://doi.org/10.1016/j.sedgeo.2015.09.004

Giant scour-fills in ancient channel-lobe transition zones: formative processes and depositional architecture

M. Hofstra[1]*, D.M. Hodgson[1], J. Peakall[1] and S.S. Flint[2]

[1] Stratigraphy Group, Department of Earth and Environment, University of Leeds, Leeds, LS2 9JT, UK

[2] Stratigraphy Group, School of Earth, Atmospheric and Environmental Sciences, University of Manchester, Manchester, Oxford Road, M13 9PL, UK

*Corresponding author: Menno Hofstra; eemh@leeds.ac.uk; phone: +44 (0) 7979 870 252 7

Co-authors emails: D.Hodgson@leeds.ac.uk; J.Peakall@leeds.ac.uk; Stephen.flint@manchester.ac.uk

Abstract

Scours are common features of modern deep-marine seascapes, particularly downstream of the mouths of slope channels within channel-lobe transition zones (CLTZs). Their dimensions can exceed hundreds of metres in width and length, and tens of metres in depth. However, the stratigraphic architecture of the infill of these erosional bedforms is rarely described from the rock record and no large (>100 m width) scours have been described in detail from exhumed CLTZs. Here, the infill of two erosional features (0.5-1 km long and 15-20 m thick) from the Permian Karoo Basin succession, South Africa, are presented from palaeogeographically well-constrained CLTZs; one from Fan 3 in the Tanqua depocentre and one from Unit A5 in the Laingsburg depocentre. The basal erosion

surfaces of the features are asymmetric with steep, undulating, and composite upstream margins, and low gradient simple downstream margins. The basal infill consists of thin-bedded siltstone and sandstone beds cut by closely-spaced scours; these beds are interpreted as partially reworked fine grained tails of bypassing flows with evidence for flow deflection. The erosional features are interpreted as giant scour-fills. The internal architecture suggests different evolutionary histories for each case. The Unit A5 scour-fill shows a simple cut-and-fill history with lateral and upward transitions from siltstone- to sandstone-prone deposits. In contrast, the Fan 3 scour-fill shows headward erosion and lengthening of the scour surface suggesting temporal changes in the interaction between turbidity currents and the scour surface. This relationship could support the occurrence of a hydraulic jump during part of the fill history, while the majority of the fill represents deposition from subcritical flows. Diversity in scour preservation mechanisms could explain the variety in depositional histories. The architecture, sedimentary facies and palaeoflow patterns of the scour-fills are distinctly different to well documented adjacent basin-floor channel-fills at the same stratigraphic levels. The recognition of scour-fills helps to constrain their sedimentological and stratigraphic expression in the subsurface, and to improve our understanding of the stratigraphic architecture of channel-lobe transition zones.

Keywords

channel-lobe transition; base-of-slope; giant scours; scour-fill; bypass; facies characteristics; Karoo Basin

1. Introduction

Large scours are readily recognised erosional bedforms on modern deep-marine seabeds (e.g., Palanques et al., 1995; Morris et al., 1998; Wynn et al., 2002a; Bonnel et al., 2005; Fildani et al., 2006; Macdonald et al., 2011a; Maier et al., 2011; Shaw et al., 2013; Covault et al., 2014; Paul et al., 2014). Commonly, these scours are concentrated within channel-lobe transition zones (CLTZs), a relatively unconfined area dominated by sediment bypass that separates the mouths of channel feeder systems from lobes (Mutti and Normark, 1987, 1991; Kenyon et al., 1995; Wynn et al., 2002a). Scours commonly form fields consisting of many individual and coalesced scours (e.g., Wynn et al., 2002a; Macdonald et al., 2011a; Shaw et al., 2013). The occurrence of scours is commonly interpreted (Komar, 1971; Mutti and Normark, 1987, 1991; Garcia and Parker, 1989; Garcia, 1993; Macdonald et al., 2011a; Ito et al., 2014), and occasionally demonstrated (Sumner et al., 2013), to be related to flows that have undergone a hydraulic jump (transformation from supercritical to subcritical flow conditions), triggered by changes in flow velocity and/or density. These changes in flow behaviour are predicted to occur in base-of-slope to basin floor transitions where there are abrupt change in gradient and degree of confinement (e.g. Alexander et al., 2008; Ito et al., 2008).

While observations of small-scale scours and megaflutes in ancient systems are abundant (e.g. Macdonald et al., 2011a), large-scale

features are not well documented. Megascours associated with Mass Transport Deposits (MTDs) have been constrained by various seismic examples (e.g., Moscardelli, 2006; Sawyer et al., 2009; Ortiz-Karpf et al., 2015) on slope settings and in some outcrop examples from lower slope to base-of-slope deposits (Pickering and Hilton, 1998, their Fig.63; Lee et al., 2004; Dakin et al., 2012). In these cases, erosional depressions are tens of metres deep and filled with chaotic deposits. In contrast, large scour-fills in turbidite systems are rarely identified in outcrop, therefore their evolution and architecture are poorly constrained. Dimensions of turbidite-filled scours reported from outcrop-related studies include the Ross Formation (Ireland) with typical dimensions of 0.3-3.5 m in depth and 1 to 45 m in length (Chapin et al., 1994; Elliott, 2000a, 2000b; Lien et al., 2003; Macdonald et al., 2011b), the Albian Black Flysch (Spain) with 1-5 m deep 5-50 m wide scours (Vicente-Bravo and Robles, 1995), the Cerro Toro Formation (Chile) with scour depths of metres and widths of tens of metres (Winn and Dott, 1979; Jobe et al.,2009) and the Windermere Group with scours up to several decimetres deep and several tens of centimetres to many tens of metres wide (Terlaky et al., 2015); composite scours up to several metres deep are reported in the Macigno Costiero Fm., Italy (Eggenhuisen et al., 2011) and the Boso Pensinsula (Japan) with erosional features filled with backset bedding up to 140 m wide and 10 m deep (Ito et al., 2014). These dimensions are an order of magnitude smaller than the scour dimensions described from modern systems (> 10 m depth and > 100 m width) (e.g. Wynn et al.,

2002a; Macdonald et al., 2011a). Scour-fills may be underrepresented in the rock record because outcrop limitations mean that they may have been misidentified as channel-fills due to cross-sectional similarity (Mutti and Normark, 1987, 1991; Wynn et al., 2002a; Normark et al., 2009). Furthermore, the stratigraphic expression of the CLTZ, including scour-fills, is rarely fully exposed or well-constrained in ancient systems (Mutti and Normark, 1987, 1991; Gardner et al., 2003; Ito et al., 2014; van der Merwe et al., 2014).

Here, the morphology and depositional architecture of two exhumed large-scale erosional scours from the Permian succession of the Karoo Basin, South Africa, are described in detail: one example from Fan 3 of the Tanqua depocentre and the other from Unit A within the Laingsburg depocentre. Previous mapping has constrained the palaeogeographic context of both locations to areas where there is a down-dip architectural change from channel- to lobe-dominated deposits (Morris et al., 2000; Van der Werff and Johnson, 2003; Sixsmith et al., 2004; Hodgson et al., 2006; Jobe et al., 2012; Prélat and Hodgson, 2013). The presented examples exhibit different sedimentological and architectural characteristics compared to basin floor channel-fills in adjacent stratigraphy. The objectives of this paper are to: i) evaluate the origin of these distinctive erosional features, ii) compare the erosional and depositional history to channel-fills, iii) develop recognition criteria for scour-fills in outcrop, iv) discuss the role of erosional bedforms in improving our understanding of the stratigraphic expression of

CLTZs within ancient submarine systems, and v) aid investigations into the role of hydraulic jumps in deep-water bedform development. Accurate recognition and description of large-scale erosional architectural elements has important implications for the robust application of outcrop studies to improve reservoir models and reduce uncertainty in subsurface investigations.

2. Regional Setting

The Karoo Basin is one of a number of Late Palaeozoic to Mesozoic basins that formed at the southern margin of Gondwana (De Wit and Ransome, 1992; Veevers et al., 1994; López-Gamundi and Rossello, 1998). The Karoo Basin has been interpreted traditionally as a retroarc foreland basin withsubsidence purely caused by the loading of the Cape Fold Belt (e.g., Johnson, 1991; Cole, 1992; Visser, 1993; Veevers et al., 1994; Catuneanu et al., 1998). More recent interpretations suggest that subsidence during the Permian was caused by dynamic topography effects due to subduction (Tankard et al., 2009) in a pre-foreland basin stage. The southwest Karoo Basin is subdivided into the Laingsburg and the Tanqua depocentres (Fig. 1) of which the deepwater fill of both depocentres is represented by the Ecca Group. The Ecca Group (Fig. 2) comprises a 2 km-thick shallowing-upward succession from distal basin-floor through submarine slope to shelf-edge and shelf deltaic settings (Wickens, 1994; Flint et al., 2011).

2.1 Tanqua depocentre

This study focuses on part of Fan 3 of the Skoorsteenberg Formation, which is one of four sand-rich basin-floor fan systems (Fig. 2) (Bouma and Wickens, 1991, 1994; Wickens and Bouma, 2000; Johnson et al., 2001). Fan 3 is the most extensively studied fan system of the Skoorsteenberg Formation, as it shows the most complete outcrop extent (Hodgson et al., 2006). The Fan 3 study area (Kleine Riet Fontein) is located in the southwestern corner of the Fan 3 outcrop, which is the most updip location (Fig. 1,3A). An integrated outcrop and research borehole dataset has established the isopach thickness of Fan 3, and the relative spatial and temporal distribution of sedimentary facies, architectural elements and palaeocurrents (Johnson et al., 2001; Hodgson et al., 2006; Prélat et al., 2009; Groenenberg et al., 2010). The axis of the system is located farther to the east along depositional strike in the Ongeluksriver area (Fig. 3A) and is characterised by distributive basin floor channel systems with overall palaeocurrent to the north/north-east(Van der Werff and Johnson, 2003; Sullivan et al., 2004; Hodgson et al., 2006; Luthi et al. 2006).The distributive character of the channel-systems at Ongeluksriver (Fig. 3A), the more deeply erosional character of the channelsin overlying Fan 4 and Unit 5, and the thinning to the south (Oliveira et al., 2009), all suggest that the southwestern outcrop-limit of Fan 3 is a proximal off-axis base-of-slope setting setting (Johnson et al., 2001, Van der Werff and Johnson, 2003; Luthi et al., 2006; Hodgson et al., 2006; Jobe et al., 2012). The Kleine Riet Fontein area was previously

179 studied in detail by Jobe et al. (2012) and interpreted as an area
180 receiving unconfined flows, supported by the wide spatial
181 distribution of numerous metre-scale scour features.

182 **2.2 Laingsburg depocentre**

183 The proximal basin floor system of the Laingsburg Formation is
184 divided into Units A and B (Sixsmith et al., 2004; Brunt et al., 2013)
185 (Fig.2). The 350 m thick Unit A comprises sand-prone sub-units A1-
186 A7, which are separated by regionally extensive mudstones
187 (Sixsmith et al., 2004; Flint et al., 2011; Prélat and Hodgson, 2013).
188 The studied outcrop is in the 'Wilgerhout' area within Unit A5, a 100
189 m thick and tens of km-long package of sandstones and siltstones on
190 the northern limb of the post-depositional Baviaans syncline (Figs. 1,
191 3B), close to the town of Laingsburg. Palaeogeographically, the
192 study area is located in the axis of the A5 system on the basin floor
193 (Sixsmith et al. 2004) (Fig.1). The large number of sand-rich channel-
194 fills that characterise the upper part of A5 in this area point to a
195 location close to the base-of-slope and/or close to the mouths of
196 large distributary channels (Sixsmith et al., 2004; Prélat and
197 Hodgson, 2013).

198

199 **3. Methodology and datasets**

200 Stratigraphic correlations were completed in the field using closely-
201 spaced sedimentary logs, photomontages, and walking out key
202 surfaces with a handheld GPS to construct architectural panels. In

the Fan 3 KRF study area (4.6 km^2), a total of 20 sedimentary logs was collected (Fig. 3A). More than 550 palaeocurrent measurements, primarily from ripple cross-lamination, were collected and tied to specific stratigraphic units. Due to the inherent variability in direction of ripple cross-laminations, a high number of measurements was needed and only surfaces with a clear dominant orientation were measured. The dip direction of ripple foresets was measured where possible to ensure an accurate palaeoflow direction. The main outcrop face consists of a 3.5 km long N-S depositional dip section. Several E-W orientated gullies to the east of the main outcrop face provide additional depositional strike control (Fig. 3A). Thin siltstone packages within the regional claystones between Fan 2 and Fan 3 provide local correlation datums.

Within the Wilgerhout area of Unit A5 a total of 17 sedimentary logs along a ~ 500m depositional dip (W-E) section was collected (Fig. 3B). The regional A5 to A6 mudstone (Sixsmith et al., 2004; Flint et al., 2011; Cobain et al., 2015) was used as the datum for all correlations. A total of 44 palaeocurrents was measured solely from ripple cross-laminations and give an average eastward directed palaeoflow (082°). Where the tectonic tilt was significant(> 20°) the azimuth of well exposed planar foresets was measured and restored.

Facies associations have been determined based on previous Karoo Basin studies (Johnson et al., 2001; Van der Werff and Johnson

2003; Grecula et al., 2003; Hodgson et al., 2006; Brunt et al., 2013) and extensive study of the Fan 3 and Unit A system. Bounding and erosion surfaces have been identified with the help of bed truncation and the absence of normal-grading structures at bed tops.

4. Facies associations

The deep-water deposits of the Karoo Basin show a limited grain size distribution ranging from claystone to fine-grained sandstones. Both Fan 3 and Unit A consist of mainly thin-bedded siltstones and very fine- to fine-grained sandstones. Flow conditions were interpreted from the described facies characteristics. A total of six distinct facies associations was identified based on field observations and are described in detail below.

4.1 Thick structureless sandstones (Fa1)

Thick (>1 m) fine-grained sandstone beds with little to no internal structure can form amalgamated sandstone packages up to 5 m thick and tens to hundreds metres wide/long, that are commonly tabular. Weak normal grading is observed at bed tops, where planar- and ripple-cross lamination may be preserved. Locally, bed bases and/or tops can show planar laminations and/or banding (alternating lighter and darker bands, see section 4.3). The sandstone beds can contain a minor amount of dispersed sub-angular mudclasts (Fig. 4A). Flame structures and tool (drag) marks are observed at bed bases.

These deposits are interpreted as rapid fall-out from sand rich high-density turbidity currents (Kneller and Branney, 1995; Stow and Johansson, 2002) with clasts representing traction-transported bedload (See section 4.2 and 4.3 for interpretation of planar laminated and banded intervals). Flame structures are associated with syn-depositional dewatering (Stow and Johansson, 2002).

4.2 Medium-bedded laminated sandstones (Fa2)

These medium- to thick-bedded (0.2 to 3 m thick), very fine-grained to fine-grained, sandstones show various sedimentary structures. Ripple lamination, in particular climbing ripple lamination, is abundant (25-70% of all laminated sandstones), showing high angles of climb with stoss-side preserved lamination (>45° on stoss-side preserved laminae) (Fig. 4B). Some beds show a clear upward increase in the angle of climb and proportion of stoss-side laminae preservation. Where planar lamination is present it is commonly at bed bases. Bases of thicker-bedded structured beds are sharp and the basal part, in comparison to the remaining laminated part of the bed, is commonly structureless. Bed tops always show abrupt normal grading to fine siltstone. Bed geometries can show lateral thickness variations on 10-s of metres scale.

High angles of climb and stoss-side preservation in ripple-laminated sandstones are indicative of rapid unidirectional aggradation rates (Jopling and Walker, 1968; Allen, 1973; Jobe et al., 2012; Morris et al., 2014). When sedimentation rate exceeds the rate of erosion at the ripple reattachment point, the stoss-side deposition is preserved

277 and aggradational bedforms develop (Allen, 1973). This style of
278 tractional deposition is attributed to rapid deceleration of the flow
279 and deposition from moderate-to low-concentration turbidity
280 currents (Allen, 1973; Jobe et al., 2012). The planar laminations
281 within the structured sandstones are interpreted to be deposited
282 under upper stage plane bed conditions (Allen, 1984; Talling et al.,
283 2012).

284 **4.3 Banded sandstones (Fa3)**

285 This facies association comprises medium- to thick-bedded fine-
286 grained sandstones (20 to 200 cm, on average 40 cm), with diffuse
287 laminae of over 1 cm thickness (Fig. 4C,5A2). This style of lamination
288 is characterised by an alternation between lighter and darker bands,
289 and is referred to as banded sandstones. Lighter bands are well
290 sorted and quartz-rich, whereas plant fragments and/or mudstone
291 clasts and micaceous materials are commonly found within the
292 poorly sorted darker bands. The banding is dominantly planar and
293 parallel to sub-parallel, but can be mildly wavy. Internal cm-scale
294 scour surfaces are common, as is loading at the bases of lighter
295 bands. Within thicker beds dominated by banded sandstone beds,
296 the bases are structureless and sharp.

297 Banded sandstones differ from planar-laminated sandstones due to
298 the thickness of the laminae (>1 cm), the thickness of the laminated
299 interval within individual event beds (>1 m) and the absence of any
300 major grain size differences between laminae. The observations
301 indicate highly concentrated, aggradational but fluctuating flow

conditions. These conditions are present during deposition in traction carpets under high-density turbidity currents (Lowe, 1982; Sumner et al., 2008, 2012; Talling et al., 2012; Cartigny et al., 2013) and have not been linked to a generic flow regime. This is comparable to the H2 division of Haughton et al. (2009) and the Type 2 tractional structures of Ito et al. (2014). The internal truncations that have been observed can be explained by quasi-steady behaviour within a stratified flow, however the extent and size of these truncations (up to m-scale) support more drastically waxing and waning flow behaviour. Combined with the thickness of individual beds within this facies group, these deposits support an interpretation of high aggradation rate and/or possibly long-duration of individual events.

4.4 Thin-bedded sandstones and siltstones (Fa4)

Thin (<20 cm) very fine-grained sandstones are interbedded with laminated siltstones (<1 cm to 5 cm). Ripple lamination, including low-angle climbing ripple lamination, is common within the sandstone beds. This facies group can be subdivided into 1) tabular sandstones with planar and ripple laminations (Fa4-1), and 2) lenticular sandstones and siltstones associated with numerous centimetre-scale erosion surfaces (Fa4-2; Figs. 4D, 5A1,5A4). Locally, Fa4-2 sandstone beds contain mudstone clasts (<1 cm) (Fig. 5A3) and can be associated with mudstone and siltstone clast conglomerates (max 0.5 m thick, 1-2 m long) that are clast-supported with a fine-grained sandstone matrix (Fig. 5B3). Within

Unit A5, thin (<5 cm) medium-grained, poorly sorted lenticular sandstone beds that are at least 10 m long (Fig. 5B1) are associated with Fa4-2 siltstones. The Fa4-2 siltstones of Unit A5 are thicker bedded (>3 cm) (Fig. 5B1).

The tabular bed geometry and predominance of current ripple lamination in Fa 4-1 are interpreted to indicate deposition from lower phase flow conditions within sluggish dilute turbidity currents (e.g., Allen, 1984). The occasional planar laminated sandstone indicates upper phase flow conditions (Best and Bridge, 1992) but with a transition to lower phase flow conditions due to ripple-laminated tops.

The Fa 4-2 group supports a higher energy environment compared to the FA4-1 group, which is interpreted based on the local presence of mudstone clasts and the numerous erosion surfaces. This facies association is interpreted to represent a period dominated by sediment bypass (e.g., Stevenson et al., 2015). The fine-grained siltstone deposits of the Fa4-2 group are interpreted to represent the tails of bypassing turbidity currents and continued reworking of the substrate by long lived turbidity currents, similar to channel-margin deposits (Grecula et al., 2003, Brunt et al., 2013). The mudstone clast conglomerates are interpreted as bedload material, derived from a mud-rich substrate, and therefore represent lag deposits of highly energetic bypassing turbidity currents. Sediment bypass zones can show fluctuations between depositional, erosional and bypass processes when being around the erosion-deposition

threshold (e.g., Wynn et al., 2002a; Ito et al., 2014; Stevenson et al., 2015). This facies association shares many similarities to the sediment bypass facies identified within the CLTZ's of sand-detached lobe systems in the Laingsburg area (van der Merwe et al., 2014). These fluctuations might result in the interbedding of siltstones and sandstones, including thin and lenticular medium-grained sandstone beds, and multiple erosion surfaces. The presence of unusually thick siltstone beds, and medium-grained sandstones, which are very rare in the Ecca Group, within the Unit A5 Fa4-2 facies group is evidence of localised deposition. The climbing ripple lamination within thin-bedded sandstones indicates rapid aggradation rates (Allen, 1973; Jobe et al., 2012).

4.5 Soft sediment deformed (SSD) deposits (Fa5) and claystones (Fa6)

The Fa5 facies group is represented by localised tightly folded and contorted heterolithic units (0.2-0.5 m thick) of thin-bedded siltstones and sandstones (Fig. 5B2). Fa5 represents a minor portion of the infill (<1%) and occurs only within the basal infill towards the margins of both features, and in close association with Fa4-2, rarely exceeding 2 m in length. Thick, regionally extensive units of Fa6 claystones occur as drapes to the deepwater sandstone units in both depocetres.

Due to their marginal location and limited proportions, the contorted thin bed units are interpreted to represent local remobilisations, above erosional relief. Fa 6 represents condensed

intervals of hemipelagic deposition, during periods of regional shutdown in coarse-grained sediment supply (Hodgson et al., 2006; Luthi et al., 2006; Flint et al., 2011; van der Merwe et al., 2014).

5. Depositional Architecture

Both features are defined by composite and asymmetric basal erosion surfaces that exceed the extent of the exposures (>350 m long in A5; >1000 m long in Fan 3) and incise 15-20 m into underlying deposits. The consistent palaeoflow directions of underlying and overlying deposits indicate that the updip margins are highly irregular, undulating and orientated sub-parallel to regional palaeoflow directions. The Fan 3 exposure is orientated 150-330° with a 340° average palaeoflow at this location (n = 435). The Unit A5 exposure is orientated 075-255° with a 082° average palaeoflow (n = 44). The type and distribution of sedimentary facies and internal stacking patterns differ between the two cases, and are discussed separately.

5.1 Fan 3 feature; Tanqua depocentre

The location of the Fan 3 erosional feature (Fig. 6) is in the middle of a north-south orientated outcrop of proximal off-axis deposits in the Kleine Riet Fontein area (Figs. 1, 6). Mapping of thickness, facies, and system-scale sedimentary architecture with the lack of channel-fills in this area compared to the Ongeluks river area to the south-east supports this as a proximal off-axis environment (Johnson et al.,

2001; Hodgson et al., 2006; Jobe et al., 2012) (Fig.3A). The overall palaeoflow is northwards (Fig. 7). The underlying deposits can be subdivided into a sandstone-prone package dominated by Fa2 and an overlying siltstone-prone package dominated by Fa4 (Figs. 6 and 7). A minor stratigraphic change in mean palaeoflow is identified between these two packages, from NNE (033°) to NNW (336°) (Fig. 7). The feature in the Kleine Riet Fontein area shows an erosional cut into the siltstone-prone package. All deposits within Fan 3 below the basal erosion surface of the studied feature extend beyond the study area and are therefore more laterally extensive . The basal erosion surface forms a series of metre-scale steps on the steep (max. 50°) updip southern margin (Figs. 5A5, 6). The full geometry of the northern margin is obscured, but the overall thinning of the fill suggests a low-angle confining surface (Fig. 6). Sedimentary sections taken towards the east (Fig. 3A) of the main N-S profile (Fig. 6) indicate eastward shallowing of the basal erosion surface and infill directed perpendicular to regional palaeoflow (Fig. 8A).

The architecture of the fill is characterised by abrupt changes in bed thickness and multiple truncation surfaces (Figs. 6, 9,10), and can be subdivided into two distinct infill packages based on changes in facies proportions and architecture across key bounding surfaces (Fig. 6, 8B). The lower package is up to 6.5m thick and is subdivided into two distinct elements (1 and 2) based on an internal truncation surface and abrupt changes in bed thickness (Fig. 6). Both elements comprise (Fig. 8B) thin-bedded siltstones and climbing ripple laminated sandstones (Fa4-2) containing small (1-4 cm) mudstone-

chips and minor (20-40 cm thick) folded thin-bedded deposits (Fa5). The lower package is only present in the northern part of the fill. The upper package is up to 12 m thick and is subdivided into five different infill elements (3-7) (Figs. 6, 9, 10) based on abrupt stratigraphic facies transitions and internal erosion surfaces. The upper package elements are predominantlymedium- to thick-bedded structured sandstones (Fig. 8B) with upward steepening climbing ripple-lamination and increased stoss-side preservation (Fa2) (Fig. 4B). Each of these elements, varying between 2 and 7.5 m in thickness, shows lateral thickness and facies changes. Within the individual elements there are no clear vertical trends, however the combination of the upper and lower packages together forms a stepped coarsening and thickening upward profile (Fig. 8B) within the axis of the feature. The lower elements in the upper package (3, 4,5) are more laterally restricted (Figs. 9,10) and show more substantial bed thickness variability compared to the upper elements (6 and 7). Element 4, and to a lesser extent element 6, thicken where the underlying elements thin (Fig. 6 and 9). Facies within the upper package are uniform with a dominance of climbing-ripple laminated sandstone (Fa2) and a transition to more thinly-bedded deposits (Fa4) towards the margins of all elements (Fig. 6) where not truncated. Elements 5 and 7 contain some banded sandstones (Fa3) directly overlying the basal erosion surface at the southern margin (Fig. 5A2), which show a northward facies transition to structureless sandstone (Fa1). Elements 3, 4 and 5 (Figs. 9 and 10) show bedsets (3-7 m thick) that comprise four to five

metre-thick (0.5 to 2.0 m) dominantly climbing-ripple laminated sandstone beds, which are interbedded with thin siltstones (<0.1 m). They are thickest near the southern margin, and pinch or taper out into thin siltstones (<5 cm) in a northward direction (over 50-150 m). Successive pinchouts occur southward, such that the beds shingle updip. Where normally graded sandstone beds thicken they amalgamate, as can be seen in element 5 (Fig. 10B). Due to accessibility issues, the exact orientation of the bedding is difficult to measure directly, but outcrop sections of element 3 and 5 (Fig. 9 and 10) indicate a shallow southward (updip) depositional dip (a few degrees). In addition, beds in element 3 dip upstream approximately 2-4° relative to the basal erosional surface (Fig. 9). Elements 6 and 7 do not preserve clear bed stacking patterns, although lateral variability in bed thickness is observed.

The palaeoflow patterns within the erosional feature in the Kleine Riet Fontein area are diverse and show lateral and stratigraphic variations. The lower package preserves a dominant south-easterly orientation (134°) within element 1 at its most southern limit, which becomes more eastward (093°) within element 2 (Fig. 6, K7). Severalhundred metres to the north, element 2 has a dominant NNE to NE (025° – K8, 035° – K9; Figs. 6 and 7) palaeoflow direction. In the upper package, there is a general NE to SE trend (096°) except for element 7, which shows an overall NE direction (028°) at its northern limit and a more NNW direction (345°) near its southernmost limit (Fig. 6). The thin-bedded deposits above the

upper package have a NNE palaeoflow (028°, n = 57), consistent with the underlying deposits and the regional trend.

A second large-scale erosional feature 800 m to the north (around K13, Fig. 3A) is situated at the same stratigraphic level in Fan 3, and shares many similarities in architecture and infill facies. The infill of this erosive feature exhibits an average NNW-directed (330°) (n=17) palaeoflow, similar to the underlying thin-bedded deposits. An irregular erosion surface(~15°) has a measured ENE orientation (070°), perpendicular to palaeoflow and overlain by structured sandstones. Three hundred metres to the east, another erosion surface (~6°) is approximately orientated NNW (335°), which is parallel to the palaeoflow, and is evident from discordance in bed dips within the thin-bedded deposits. The basal surface has a minimum length of 500 m perpendicular to palaeoflow and cuts at least 10 m into underlying deposits. Close to the western margin the fill consists solely of Fa2 facies, but eastwards where the fill thickens, it consists of a lower package of thin-bedded siltstones and sandstones (Fa4-2) and an upper package of structured sandstones (Fa2), that are locally amalgamated.

5.2 Unit A5 feature; Laingsburg depocentre

The erosional feature at Wilgerhout lies in the upper half of Unit A5 (60-70 m from the base) within a succession of stacked lobes locally cut by sand-rich channel-forms (Prélat and Hodgson, 2013). A large channel (>600 m wide and >15 m deep) filled by amalgamated structureless sandstones (Fa1) is present at the top of the A5

503 succession in this location. The association of channels and lobes in
504 this area supports a base-of-slope setting, within the upper part of
505 the Unit A5 system based on regional mapping (Sixsmith et al., 2004;
506 Prélat and Hodgson, 2013). The exposure is limited to a 1 km long E-
507 W orientated section. Regional palaeoflow patterns are towards the
508 ENE (Sixsmith et al., 2004), which is consistent with measurements
509 from the infill deposits (Fig. 11). The section shows a steep (2-50°)
510 and stepped western (updip) margin.

511 The fill consists of three distinct sedimentary packages. A lower
512 package (1.5-5 m thick) comprises thin-bedded siltstones with rare
513 banded or ripple laminated fine-grained sandstone beds (Fa4-2) (Fig.
514 11). Locally, thin (<30 cm) mudstone clast conglomerates directly
515 overlie the basal erosion surface. Multiple small-scale (<20 cm deep)
516 cross-cutting erosional surfaces incise into thin-bedded siltstones in
517 the basal ~0.5 m of the fill, but decrease towards the top. Thin (2-3
518 cm) and lenticular moderately sorted medium-grained sandstones
519 are present within the siltstones and individual normally graded
520 siltstone beds are thick (> 3 cm) (Fig. 5B1). The middle package (0.5-
521 10 m thick) comprises medium-bedded banded (Fa3) and
522 structureless sandstones (Fa1) interbedded with siltstones, which
523 pass abruptly from sandstone-dominated to siltstone-dominated
524 (Fa4-2) at the western margin (Fig. 5B4). Some minor tightly folded
525 deposits (Fa5) (Fig. 5B2) occur within the siltstone dominated
526 western margin succession. The upper package (3-8.5 m thick)
527 comprises thick-bedded sharp-based structureless partially
528 amalgamated fine-grained sandstones (Fa1) interbedded with the

occasional banded sandstone and thin-bedded siltstone (Fig. 11). This package extends beyond the limits of erosional confinement, but increases in thickness above the deepest point of the basal erosion surface. Within all three infill packages no clear vertical stratigraphic trends have been observed. However, the combination of the three infill packages together (Fig. 11B –W15) shows a step-wise coarsening- and thickening-upward trend above the basal surface. Above the upper package a 4 metre thick fining- and thinning-upwards unit can be observed (Fig. 11) from thick- to medium-bedded dominantly structureless sandstones (Fa1) to thin-bedded sandstone and siltstone deposits (Fa 4). As these deposits are tabular, they are not considered to be part of the fill. Up to 500 m west (updip) of the basal erosional surface at the same stratigraphic level, a fine-grained thin-bedded package (1-2 m thick) is characterised by multiple small-scale (10-20 cm) erosion surfaces, thin sandstone beds, and abrupt bed thickness changes.

6. Discussion

6.1 Origin and infill of erosional features

The average palaeocurrents from underlying and overlying deposits indicate that the large asymmetric erosion surfaces described from Fan 3 (Tanqua) and Unit A5 (Laingsburg) are dip-sections (Figs. 3, 6,11). The steeper upstream surfaces dip at angles of 4-50° (Fan 3) and 2-50° (Unit A5), with prominent metre-scale steps and multiple erosion surfaces indicating the composite nature of the basal

surface. In the Kleine Riet Fontein area (Fan 3), the transverse to downstream section is shallow (~3.5°) and smooth (Fig. 6), and shows prominent asymmetry in three dimensions with shallowing of the basal surface perpendicular to the regional palaeoflow (Fig. 10A). Palaeocurrents within the basal are diverse and at a high angle (orientated N to SE) to underlying and overlying deposits (orientated NNW), with palaeoflow differences of up to 180° (Fig. 7).

An asymmetric and composite basal erosional surface with stacked smaller-scale elements could support an interpretation of a sinuous submarine channel-fill. However, in a cut through a sinuous channel-fill the palaeocurrents would be expected to be dominantly parallel to channel banks (dip sections) (Parsons et al., 2010; Wei et al., 2013; Sumner et al., 2014) and are only rarely described at high angles to the basal surface (Pyles et al., 2012). Known exhumed examples of outer bank deposits have relatively higher energy facies such as conglomerates, and coarse-grained and/or amalgamated sandstones (e.g., Young et al., 2003; Labourdette et al., 2007; Hodgson et al., 2011; Janocko et al., 2013) compared to inner bank deposits, which does not match with the observed distribution of facies and the relatively low-energy character of the Kleine Riet Fontein infill. Furthermore, channel sinuosity is predicted to be low for the slope gradients of base-of-slope and basin-floor channel bends (e.g., Clark et al., 1992 – close to 1.0 sinuosity at 1:1000 slope angles), especially in sand-prone systems without levees and at mid-high palaeolatitudes (50-60°S) at which the Karoo system formed (Peakall et al., 2012, 2013; Morris et al., 2014; Cossu et al., 2015).

Consequently, given the low predicted sinuosities it is unlikely that channel bend facies would be at high angles to the regional slope. In contrast, the morphology of the basal surface, the palaeocurrent pattern, and distribution of sedimentary facies support an interpretation of large-scale scour-fills, with prominent steep headwalls and lower-angle downstream margins. In addition, coarsening- and thickening-upwards trends as identified within both features, considering the complete infill, are more readily explained as a progradational trend (e.g., Macdonald et al., 2011b) than channel-fills. Basin-floor channel-fills in the Ecca Group have been described by several authors (e.g., Johnson et al., 2001; Sixsmith et al., 2004; Sullivan et al., 2004; Brunt et al., 2013), and are dominantly characterised by structureless sandstone, highly amalgamated in the axis of the fills and more thin-bedded towards the margins and top of the fills . Where well preserved, the basal erosion surface and facies distribution of basin-floor channels are symmetrical (Sullivan et al., 2004; Luthi et al., 2006), and typically ~250-350 m wide and 15-20 m thick (Pringle et al., 2010; Brunt et al., 2013). The large-scale scour-fills described, therefore, are distinctly different to the published examples of basin-floor channel fills from the Karoo Basin in terms of their architecture, facies types and distributions, and relationship of palaeoflow to the bounding surface, as well as to sinuous channels from other settings. The erosional feature within the Kleine Riet Fontein area of Fan 3 has been previously interpreted as a channel-fill. Morris et al. (2000) classified it as a crevasse channel-fill, while Van der Werff and

606 Johnson (2003) interpreted it as the distal depositional part of an
607 overbank channel-fill with a SE-NW orientation. Implicit in both
608 interpretations was that the depositional architecture is different to
609 the basin-floor channel-fills at the same stratigraphic level 7-8 km to
610 the east (e.g., Sullivan et al., 2004; Luthi et al., 2006).

611 The basal fine-grained fill (Fa4-2) in both scour-fills is interpreted to
612 indicate sediment bypass and the deposition of low-energy tails of
613 flows. The interpretation of thin-bedded deposits indicating
614 sediment bypass has been previously made for channel-fills (e.g.,
615 Beaubouef and Friedmann, 2000; Grecula et al., 2003; Brunt et al.,
616 2013; Stevenson et al., 2015). However the thicknesses of individual
617 siltstone beds (>3 cm) within the Unit A5 fill is distinctive, and is
618 interpreted to reflect the capture of flow tails in a scour depression,
619 in a similar manner to thick siltstones in internal levee successions
620 (Kane and Hodgson, 2011). In the Kleine Riet Fontein feature (Fan 3),
621 the diverse palaeoflow directions in the basal siltstone units
622 suggests deflection and spreadingl of flow at the upstream end.
623 Complex flow patterns are known to be associated with flutes and
624 scours (e.g., Eggenhuisen et al., 2011) with flows exhibiting a
625 recirculating separation cell that forms downstream of the scour lip
626 as the basal high velocity part of the flow is jetted over the
627 depression (Allen, 1971; Farhoudi and Smith, 1985; Karim and Ali,
628 2000). This may occur in both subcritical and supercritical flows.
629 When the palaeoflow patterns of element 2 (at K7, K8, and K9) are
630 compared with the streamline patterns of the spindle-shaped
631 erosional marks of Allen (1971), and assuming a scour orientated

with the flow direction of the underlying deposits (336°), there is a close fit in terms of variance and spread (Fig. 12). Therefore, the observed palaeoflow patterns can be explained by the presence of a flow separation cell and the generation of reversed bedload transport at the bottom of the flow when passing through the depression (Fig. 12).

The second erosional feature located 800 m downstream of the Kleine Riet Fontein scour is similar in architecture and fill. It shows erosion and downcutting surfaces both perpendicular (10° cut to 330° palaeoflow) and parallel (335° cut to 330° palaeoflow) to regional palaeoflow. The morphology suggests this second erosional feature is also a large composite scour-fill (>300 m wide). As this northern scour is atthe same stratigraphic level, it indicates there may be a larger area of erosional bedforms present. This fits with the interpretations of Jobe et al. (2012) defining the Kleine Riet Fontein area as an area receiving unconfined flows. A spatial distribution of multiple scour-fills in this proximal off-axis area adjacent to distributive channels in Ongeluks River (Fig. 3) supports the interpretation of a channel-lobe transition zone close to the base-of-slope.

6.2 Flow-scour dynamics

The merging of multiple erosion surfaces at the steep and stepped upstream margin of both scour-fills point to their composite origin, with multiple flows shaping the morphology of the basal surface. The basal successions of both scour-fills are similar. However, bed

architecture, stacking patterns, erosion surfaces, and facies of the upper elements (3-7) in the Kleine Riet Fontein featurepoint to a more complicated interaction between flow and seabed relief in a later stage of scour evolution.

In the Unit A5 feature, the irregular basal surface suggests that after initial development of the scour, the upstream margin was weakly modified, with little evidence of headward erosion. Minor internal erosion surfaces exist, but generally beds taper towards the upstream margin. The stratigraphic transition from the siltstone- to sandstone-prone deposits points to initial sediment bypass (multiple erosion surfaces and medium-grained sandstone lenses) followed by a period of aggradation (structureless Fa1 and banded sandstones Fa3) as the depression filled. The passive depositional character of these packages and the lack of supercritical bedforms, suggests a subcritical nature for the infill.

In the case of the Kleine Riet Fontein scour, the evolution of the scour is assessed from the architecture and stacking patterns of the elements (Fig. 13).. The position of the upstream margin of the scour during deposition of element 1 was downstream of the current position of element 2, being deposited after another phase of erosion, evident from the stepped basal erosional surface (Fig.6). Element 3 shows a similar southward migration after reshaping of the updip margin and only partially filled the depression. Element 4 is interpreted to have largely filled the accommodation in the downstream and lateral part of the scour. This was truncated by

another erosional event that reshaped the updip margin and removed large parts of element 2 and 3. Element 5 and 6 have slightly erosional bases, but mostly infill available accommodation by stacking in a downstream direction. Element 7 has a more uniform thickness but modified the updip margin (Figs. 6 and 13). The interpreted evolution of the basal surface suggests that the initial scouring phase(s) may not be preserved due to sequential deepening and widening of the scour.. The stacking of the elements and internal erosion surfaces in the Kleine Riet Fontein scour-fill indicate upstream migration (Fig. 13) and lengthening of the original scour surface through headward erosion. Headward erosion, or backward incision, occurs in both supercritical and subcritical flows (e.g., Izumi and Parker, 2000; Hoyal and Sheets, 2009). The sedimentary facies and bed geometries of the elements in the upper package are characterised by stoss-side preserved steep climbing-ripple dominated sandstones that indicate rapid localised fallout from relatively low-concentration turbidity currents. Climbing ripple lamination extends across almost the whole length of the scour-fill until in close proximity of the upstream head of the scour. The shallow (a few degrees) upstream depositional dip observed in a number of the infill elements (3, 4, 5)resemble backset bedding (Fig. 9). Backset bedding has been linked to abrupt changes in confinement (Ito et al., 2014), associated with the occurrence of a hydraulic jump (Jopling and Richardson, 1966; Lang and Winsemann, 2013; Cartigny et al., 2014; Ito et al. 2014). The backset deposits, and the majority of the scour-fill, are characterised almost

exclusively by climbing ripple-lamination (Fa 2).These deposits may be either the product of rapid settling from the downstream parts of hydraulic jumps as the scour migrated headward, or the products of subsequent infill by subcritical currents after being previously cut by flows that underwent a hydraulic jump. The measurements of hydraulic jumps over giant scours in a natural gravity current demonstrate, however, that the hydraulic jump enhances upward fluid movement for large distances downstream of the hydraulic jump (Sumner et al., 2013), and therefore minimises sedimentation within the scour. Additionally, the presence of climbing ripple lamination very close to the head of the scour suggests that this final phase was the product of depositional subcritical flows. In combination with the lack of evidence for any depositional features typical of supercritical conditions (supercritical bedforms), other than the backset bedding in elements 3-5, this suggests that the predominant fill of the scour was by subcritical flows. Thus the inception, deepening, and sediment bypass phases of these giant scours may well have been associated with hydraulic jumps in supercritical flows, whilst their infill was dominantly the product of later subcritical flows. This contrasts to the supercritical deposits interpreted in other examples of backset bedding (Jopling and Richardson, 1966; Lang and Winsemann, 2013; Cartigny et al., 2014; Ito et al., 2014).

The infill character of the scour to the north of the main Kleine Riet Fontein scour is very similar, with a lower siltstone-prone package and an abrupt change into an upper climbing-ripple dominated

734 sandstone package. This suggests both features share a similar
735 depositional history, which could be due to an internal control
736 linked to an updip avulsion or an external control such as a
737 substantial change in turbidity current energy and/or size. Existing
738 local seabed depressions consisting of partially filled scours could
739 have triggered hydraulic jumps and subsequently reshaped their
740 morphology in a similar manner in both scours, followed by lower
741 energy subcritical flows, explaining the similarity in infill character.

742 **6.3 Preservation of giant scour-fills**

743 Within scour fields in modern systems, amalgamation or
744 coalescence of scours is a common phenomenon (e.g., Parker, 1982;
745 Macdonald et al., 2011a; Fildani et al., 2013; Shaw et al., 2013). It
746 has been emphasized that changes in the behaviour of flows as they
747 pass over the erosional relief of small-scale scours leads to the
748 development of larger depressions (e.g., Shaw et al., 2013). This
749 could be due either to the development of flow separation zones,
750 enhancing erosion, or to the triggering of a hydraulic jump (Sumner
751 et al., 2013). A gap remains, however, in scale between scours
752 documented from the modern seabed and megaflutes and scours
753 interpreted from outcrop studies (Fig. 14). Exhumed scours of the
754 scale described here, and filled with turbidites, have not been
755 described in detail previously. However, the scale of these scour-fills
756 coincides with the range known from modern-day scours (Fig. 14) in
757 CLTZs (e.g., Kenyon et al., 1995; Wynn et al., 2002a; Macdonald et
758 al., 2011a). Due to their composite character and upstream

759 migration, these scour bodies are able to reach significant
760 dimensions. This study shows that within sand-rich turbidite
761 systems, such as in the Karoo Basin, scour-fills of dimensions
762 documented from modern system can be expected to be preserved,
763 and care is needed to discriminate them from submarine channel-
764 fills.

765 Possible explanations for the preservation of large-scale composite
766 scour-fills within CLTZs include i) large scale avulsion of the main
767 feeder system prior to channel propagation into the scoured CLTZ
768 area, ii) the presence of scours at the maximum extent of channel
769 propagation into the basin, and/or iii) lateral position during channel
770 progradation. Differences can however be expected in the character
771 of scour fills between the different preservation mechanisms (Fig.
772 15). As CLTZ's are known to be extensive and widespread areas (in
773 modern systems ~500km - >10,000 km^2) (Wynn et al., 2002a) and
774 channel systems are limited in cross-sectional dimensions, it implies
775 that not all scour remnants, including larger coalescent ones, will be
776 reworked by a period of channel propagation (Macdonald et al.,
777 2011a) through a lobe environment (Jegou et al., 2008; Macdonald
778 et al., 2011b; Morris et al., 2014). In the case of a channel
779 progradation adjacent to the scour, the infill signal will depend on
780 the nature of the channel (A1 and B1). In the case the channel is
781 purely erosionally confined (A1), it is expected to show a coarsening-
782 and thickening-upward profile due to the sand-rich nature of
783 overbank deposits (Johnson et al., 2001;Grecula et al., 2003; Van der
784 Werff et al., 2003; Brunt et al., 2012). Progradation of a levee-

confined (B1) system could however lead to the reverse infill pattern, as more fine-grained (levee) materials would be deposited inside the scour when the channel-levee system matures. In the case of maximum channel progradation (B2), the overall initial sedimentary signal would be coarsening- and thinning upwards as the scour would have been filled by axial lobe sands during retrogradation. In the case of avulsion of the main feeder channel before complete fill of the scour, the depositional signal would be characterized by a fining- and thinning profile as fringe materials from adjacent lobes are likely to be deposited within the abandoned scours. As the infill signal of both examples here presented fit with infill signal A (coarsening- and thickening-upward) of Figure 15, their depositional history is most likely related to (one of) the two presented preservation mechanisms (B1 and B2).

7. Conclusions

This study reports the first detailed documentation of exhumed giant (>1000-1500 m long) turbidite-filled scours from ancient deep-marine settings. Palaeogeographically, both scour-fills are constrained to base-of-slope channel-lobe transition zone settings. The scour-fills exhibit composite and downstream assymetric basal erosion surfaces, with internal erosion surfaces and, in one case, evidence for extensive headward erosion. The sedimentary infills show stepped coarsening- and thickening-upwards trends, with the basal fine-grained deposits being associated with low-energy tails of bypassing turbidity currents and subsequent reworking. Palaeoflow

patterns within the Fan3 Kleine Riet Fontein scour indicate complicated deflected flow patterns, which supports interpretation of headward recirculation and downstream flow expansion. The simple infill architecture of the Unit A5 scour suggests a rather straightforward cut-and-fill history. The facies and architecture of the Fan 3 Kleine Riet Fontein scour-fill, however, points to a more dynamic history of interactions between flows and the relief of the scour, resulting in a more complicated architecture with evidence for headward erosion and a series of large internal erosion surfaces. The contrast in depositional architecture of the two scour-fills demonstrates that these erosional bedforms can develop diverse depositional histories, presumably as a function of the interaction between the character of the turbidity currents and evolving geometry of the scour surfaces. The steep updip margins, stepped coarsening- and thickening upward successions of dominantly subcritical flow deposits, and internal palaeocurrent dispersal patterns contrast with laterally and stratigraphically adjacent basin-floor channel-fills. Despite their palaeogeographic setting and evidence for formation by hydraulic jumps, their fills, including backset deposits, do not correspond with deposition from supercritical flows. Documenting the facies and architecture of scour-fills is important for the identification and description of areas dominated by sediment bypass in the rock record, and has consequences for the accurate geological modelling of CLTZs.

Acknowledgements

This work was carried out as part of the LOBE 2 consortium research project. We are grateful for the financial support from: Anadarko, Bayerngas Norge, BG Group, BHP Billiton, BP, Chevron, Dong Energy, E.ON, GDF Suez, Maersk Oil, Marathon Oil, Shell, Statoil, Total, VNG Norge, and Woodside. We also acknowledge the landowners from both the Tanqua and the Laingsburg areas for access to their land. Finally, Renée de Bruijn and Nienke Lips are thanked for their assistance in the field.

References

Alexander, J., McLelland, S.J., Gray, T.E., Vincent, C.E., Leeder, M.R., Ellett, S., 2008. Laboratory sustained turbidity currents form elongate ridges at channel mouths. Sedimentology 55, 845-868.

Allen, J.R.L., 1971. Transverse erosional marks of mud and rock: their physical basis and geological significance. Sedimentary Geology 5, 167-385.

Allen, J.R.L., 1973. A classification of climbing-ripple cross-lamination. Journal of the Geological Society of London 129, 537-541.

Allen, J.R.L., 1984. Parallel lamination developed from upper-stage plane beds: a model based on the larger coherent structures of the turbulent boundary layer. Sedimentary Geology 39, 227-242.

Beaubouef, R., Friedmann, S., 2000. High resolution seismic/sequence stratigraphic framework for the evolution of Pleistocene intra slope basins, western Gulf of Mexico: depositional models and reservoir analogs. In: Weimer, P., Slatt, R.M., Coleman, J., Rosen, N.C., Nelson, H., Bouma, A.H., Styzen, M.J., Lawrence, D.T. (Eds.), Deep Water Reservoirs of the World. GCSSEPM Foundation, Houston, pp. 40-60.

Best, J., Bridge, J., 1992. The morphology and dynamics of low amplitude bedwaves upon upper stage plane beds and the preservation of planar laminae, Sedimentology 39, 737-752.

866 Bonnel, C., Dennielou, B., Droz, L., Mulder, T., Berné, S., 2005.
867 Architecture and depositional pattern of the Rhône Neofan and
868 recent gravity activity in the Gulf of Lions (western Mediterranean).
869 Marine and Petroleum Geology 22, 827-843.

870 Bouma, A.H., Wickens, H.deV., 1991. Permian passive margin
871 submarine fan complex, Karoo basin, South Africa: possible model to
872 Gulf of Mexico. Gulf Coast Association of Geological Societies
873 Transactions 41, 30-42.

874 Bouma, A.H., Wickens, H.deV., 1994. Tanqua Karoo, ancient analog
875 for fine-grained submarine fans. In: Weimer, P., Bouma. A.H.,
876 Perkins, B.F. (Eds.), Submarine Fans and Turbidite Systems:
877 Sequence Stratigraphy, Reservoir Architecture, and Production
878 Characteristics. Gulf Coast Section SEPM Foundation 15th Research
879 Conference Proceedings, pp. 23-34.

880 Brunt, R.L., Hodgson, D.M., Flint, S.S., Pringle, J.K., Di Celma, C.,
881 Prélat, A., Grecula, M., 2013. Confined to unconfined: Anatomy of a
882 base of slope succession, Karoo Basin, South Africa. Marine and
883 Petroleum Geology 41, 206-221.

884 Cartigny, M.J., Eggenhuisen, J.T., Hansen, E.W., Postma, G., 2013.
885 Concentration-dependent flow stratification in experimental high-
886 density turbidity currents and their relevance to turbidite facies
887 models. Journal of Sedimentary Research 83, 1047-1065.

888 Cartigny, M.J., Ventra, D., Postma, G., Den Berg, J.H., 2014.
889 Morphodynamics and sedimentary structures of bedforms under

890 supercritical-flow conditions: New insight from flume experiments.
891 Sedimentology 61, 712-748.

892 Catuneanu, O., Hancox, P., Rubidge, B., 1998. Reciprocal flexural
893 behaviour and contrasting stratigraphies: a new basin development
894 model for the Karoo retroarc foreland system, South Africa. Basin
895 Research 10, 417-439.

896 Chapin, M., Davies, P., Gibson, J., Pettingill, H., 1994. Reservoir
897 architecture of turbidite sheet sandstones in laterally extensive
898 outcrops, Ross Formation, western Ireland. In: Weimer, P., Bouma,
899 A.H., Perkins, B.F. (Eds.), Submarine Fans and Turbidite Systems:
900 Sequence Stratigraphy, Reservoir Architecture, and Production
901 Characteristics. Gulf Coast Section SEPM Foundation 15th Research
902 Conference Proceedings, pp. 53-68.

903 Clark, J.D., Pickering, K.T., 1996. Submarine channels; Processes and
904 Architecture, Vallis Press, London, 231 p.

905 Clark, J.D., Kenyon, N.H., Pickering, K.T., 1992. Quantitative analysis
906 of the geometry of submarine channels: implications for
907 classification of submarine fans. Geology 20, 633-636.

908 Cobain, S.L., Peakall, J., Hodgson, D.M., (2015). Indicators of
909 propagation direction and relative depth in clastic injectites:
910 implications for laminar versus turbulent flow processes. GSA
911 Bulletin. DOI:10.1130/B31209.1

912 Cole, D., 1992. Evolution and development of the Karoo Basin. In: De
913 Wit, M.J., Ransome, I.G.D. (Eds.), Inversion Tectonics of the Cape

914 Fold Belt, Karoo and Cretaceous Basins of Southern Africa. Balkema,
915 Rotterdam, pp. 87-99.

916 Cossu, R., Wells, M.G., Peakall, J., 2015. Latitudinal variations in
917 submarine channel sedimentation patterns: the role of the Coriolis
918 forces. Journal of the Geological Society 172, 161-174.

919 Covault, J.A., Kostic, S., Paull, C.K., Ryan, H.F., Fildani, A. 2014.
920 Submarine channel initiation, filling and maintenance from sea-floor
921 geomorphology and morphodynamic modelling of cyclic steps.
922 Sedimentology 61, 1031-1054.Dakin, N., Pickering, K.T., Mohrig, D.,
923 Bayliss, N.J., 2012. Channel-like features created by erosive
924 submarine debris flows: Field evidence from the Middle Eocene
925 Ainsa Basin, Spanish Pyrenees. Marine and Petroleum Geology 41,
926 62-71.

927 De Wit, M.J., Ransome, I.G., 1992. Regional inversion tectonics along
928 the southern margin of Gondwana. In: De Wit, M.J., Ransome, I.G.D.
929 (Eds.), Inversion Tectonics of the Cape Fold Belt, Karoo and
930 Cretaceous Basins of Southern Africa. Amsterdam, Balkema, pp. 15-
931 22.

932 Eggenhuisen, J.T., McCaffrey, W.D., Haughton, P.D., Butler, R.W.
933 2011. Shallow erosion beneath turbidity currents and its impact on
934 the architectural development of turbidite sheet systems.
935 Sedimentology 58, 936-959.

936 Elliott, T., 2000a. Depositional architecture of a sand-rich,
937 channelized turbidite system: the Upper Carboniferous Ross

938 Sandstone Formation, western Ireland. In: Weimer, P., Slatt, R.M.,
939 Coleman, J., Rosen, N.C., Nelson, H., Bouma, A.H., Styzen, M.J.,
940 Lawrence, D.T. (Eds.), Deep Water Reservoirs of the World.
941 GCSSEPM Foundation, Houston, pp. 342-373.

942 Elliott, T., 2000b. Megaflute erosion surfaces and the initiation of
943 turbidite channels. Geology 28, 119-122.

944 Farhoudi, J., Smith, K.V., 1985. Local scour profiles downstream of
945 hydraulic jump. Journal of Hydraulic Research 23, 343-358.

946 Fildani, A., Normark, W.R., Kostic, S., Parker, G. 2006. Channel
947 formation by flow stripping: Large-scale scour features along the
948 Monterey East Channel and their relation to sediment waves.
949 Sedimentology 53, 1265-1287.

950 Fildani, A., Hubbard, S.M., Covault, J.A., Maier, K.L., Romans, B.W.,
951 Traer, M., Rowland, J.C., 2013. Erosion at inception of deep-sea
952 channels. Marine and Petroleum Geology 41, 48-61.

953 Flint, S.S., Hodgson, D.M., Sprague, A., Brunt, R.L., Van der Merwe,
954 W.C., Figueiredo, J., Prélat, A., Box, D., Di Celma, C., Kavanagh, J.P.,
955 2011. Depositional architecture and sequence stratigraphy of the
956 Karoo basin floor to shelf edge succession, Laingsburg depocentre,
957 South Africa. Marine and Petroleum Geology 28, 658-674.

958 Garcia, M.H. 1993. Hydraulic jumps in sediment-driven bottom
959 currents. Journal of Hydraulic Engineering 119, 1094-1117.

960 Garcia, M., Parker, G., 1989. Experiments on hydraulic jumps in
961 turbidity currents near a canyon-fan transition. Science 245, 393-
962 396.

963 Gardner, M.H., Borer, J.M., Melick, J.J., Mavilla, N., Dechesne, M.,
964 Wagerle, R.N., 2003. Stratigraphic process-response model for
965 submarine channels and related features from studies of Permian
966 Brushy Canyon outcrops, West Texas. Marine and Petroleum
967 Geology 20, 757-787.

968 Grecula, M., Flint, S.S., Wickens, H.DeV., Johnson, S.D., 2003.
969 Upward-thickening patterns and lateral continuity of Permian sand-
970 rich turbidite channel fills, Laingsburg Karoo, South Africa.
971 Sedimentology 50, 831-853.

972 Groenenberg, R.M., Hodgson, D.M., Prélat, A., Luthi, S.M., Flint, S.S.,
973 2010. Flow-deposit interaction in submarine lobes: insights from
974 outcrop observations and realizations of a process-based numerical
975 model. Journal of Sedimentary Research 80, 252-267.

976 Haughton, P., Davis, C., McCaffrey, W., Barker, S., 2009. Hybrid
977 sediment gravity flow deposits-classification, origin and significance.
978 Marine and Petroleum Geology 26, 1900-1918.

979 Hodgson, D.M., Flint, S.S., Hodgetts, D., Drinkwater, N.J.,
980 Johannessen, E.P., Luthi, S.M., 2006. Stratigraphic evolution of fine-
981 grained submarine fan systems, Tanqua Depocenter, Karoo Basin,
982 South Africa. Journal of Sedimentary Research 76, 20-40.

983 Hodgson, D.M., Di Celma, C.N., Brunt, R.L., Flint, S.S., 2011.
984 Submarine slope degradation and aggradation and the stratigraphic
985 evolution of channel-levee systems. Journal of the Geological
986 Society of London 168, 625-628.

987 Hoyal, D.C.J.D., Sheets, B.A. 2009. Morphodynamic evolution of
988 experimental cohesive deltas. Journal of Geophysical Research:
989 Earth Surface 114, 2003-2012.

990 Ito, M., 2008. Downfan transformation from turbidity currents to
991 debris flows at a channel-to-lobe transitional zone: the lower
992 Pleistocene Otadai Formation. Journal of Sedimentary Research 78,
993 668-682.

994 Ito, M., Ishikawa, K., Nishida, N., 2014. Distinctive erosional and
995 depositional structures formed at a canyon mouth: A lower
996 Pleistocene deep-water succession in the Kasuza forearc basin on
997 the Boso Peninsula, Japan. Sedimentology 61, 2042-2062.

998 Izumi, N., Parker, G., 2000. Linear stability analysis of channel
999 inception: downstream-driven theory. Journal of Fluid Mechanics
1000 419, 239-262.

1001 Janocko, M., Nemec, W., Henriksen, S., Warchol, M., 2013. The
1002 diversity of deep-water sinuous channel belts and slope valley-fill
1003 complexes. Marine and Petroleum Geology 41, 7-34.

1004 Jegou, I., Savoye, B., Pirmez, C., Droz, L., 2008. Channel-mouth lobe
1005 complex of the recent Amazon Fan: The missing piece. Marine
1006 Geology 252, 62-77.

1007 Jobe, Z.R., Lowe, D.R., Morris, W.R., 2012. Climbing-ripple
1008 successions in turbidite systems: depositional environments,
1009 sedimentation rates and accumulation times. Sedimentology 59,
1010 867-898.

1011 Jobe, Z.R., Bernhardt, A., Fosdick, J.C., Lowe, D.R., 2009. Cerro Toro
1012 channel margins, Sierra del Toro. In: Fildani, A., Hubbard, S.M.,
1013 Romans, B.W. (Eds.). Stratigraphic Evolution of Deep-Water
1014 Architecture: Examples of Controls and Depositional Styles from the
1015 Magallanes Basin, Southern Chile 2009. SEPM Field Trip Guidebook
1016 10, pp. 31-33.

1017 Johnson, M., 1991. Sandstone petrography, provenance and plate
1018 tectonic setting in Gondwana context of the southeastern Cape-
1019 Karoo Basin. South African Journal of Geology 94, 137-154.

1020 Johnson, S.D., Flint, S.S., Hinds, D., Wickens, H.DeV., 2001. Anatomy,
1021 geometry and sequence stratigraphy of basin floor to slope turbidite
1022 systems, Tanqua Karoo, South Africa. Sedimentology 48, 987-1023.

1023 Jopling, A. V., Richardson, E. V., 1966. Backset bedding developed in
1024 shooting flow in laboratory experiments: NOTES. Journal of
1025 Sedimentary Research 36, 821-825.

1026 Jopling, A.V., Walker, R.G. 1968. Morphology and origin of ripple-
1027 drift cross-lamination, with examples from the Pleistocene of
1028 Massachusetts. Journal of Sedimentary Research 38, 971-984.

1029 Kane, I.A., Hodgson, D.M., 2011. Sedimentological criteria to
1030 differentiate submarine channel levee subenvironments: exhumed

1031 examples from the Rosario Fm. (Upper Cretaceous) of Baja
1032 California, Mexico, and the Fort Brown Fm. (Permian), Karoo basin,
1033 S. Africa. Marine and Petroleum Geology 28, 807-823.

1034 Karim, O., Ali, K., 2000. Prediction of flow patterns in local scour
1035 holes caused by turbulent water jets. Journal of Hydraulic Research
1036 38, 279-287.

1037 Kenyon, N.H., Millington, J., Droz, L., Ivanov, M.K., 1995. Scour holes
1038 in a channel-lobe transition zone on the Rhône Cone. In: Pickering,
1039 K.T., Hiscott, R.N., Kenyon, N.H., Ricci-Lucchi, F., Smith, R.D.A (Eds),
1040 Atlas of Deep Water Environments; Architectural Style in Turbidite
1041 Systems. Chapman & Hall, London, pp. 212-215.

1042 Kneller, B.C., Branney, M.J., 1995. Sustained high-density turbidity
1043 currents and the deposition of thick massive sands. Sedimentology
1044 42, 607-616.

1045 Komar, P.D., 1971. Hydraulic Jumps in turbidity currents. Geological
1046 Society of America Bulletin 82, 1477.

1047 Labourdette, R. 2007., Integrated three-dimensional modelling
1048 approach of stacked turbidite channels. AAPG bulletin 91, 1603-
1049 1618.

1050 Lang, J., Winsemann, J., 2013. Lateral and vertical facies
1051 relationships of bedforms deposited by aggrading supercritical
1052 flows: from cyclic steps to humback dunes. Sedimentary Geology
1053 296, 36-54. Lee, S.E., Amy, L.A., Talling, P.J., 2004. The character and
1054 origin of thick base-of-slope sandstone units of the Peïra Cava

outlier, SE France. In: Joseph, P., Lomas, S.A. (Eds.), Deep-Water Sedimentation in the Alpine Foreland Basin of SE France: New Perspectives on the Grès d'Annot and Related Systems. Geological Society London, Special Publications 221, pp. 331-347.

Lien, T., Walker, R.G., Martinsen, O.J., 2003. Turbidites in the Upper Carboniferous Ross Formation, western Ireland: reconstruction of a channel and spillover system. Sedimentology, 50, 113-148.

Lòpez-Gamundi, O.R., Rossello, E.A., 1998. Basin fill evolution and paleotectonic patterns along the Samfrau geosyncline: the Sauce Grande basin-Ventana foldbelt (Argentina) and Karoo basin-Cape foldbelt (South Africa) revisited. Geologische Rundschau 86, 819-834.

Lowe, D.R., 1982. Sediment gravity flows: II Depositional models with special reference to the deposits of high-density turbidity currents. Journal of Sedimentary Research 52, 279-297.

Luthi, S.M., Hodgson, D.M., Geel, C.R., Flint, S.S., Goedbloed, J.W., Drinkwater, N.J., Johannessen, E.P., 2006. Contribution of research borehole data to modelling fine-grained turbidite reservoir analogues, Permian Tanqua–Karoo basin-floor fans (South Africa). Petroleum Geoscience 12, 175-190.

Macdonald, R.G., Alexander, J., Bacon, J.C., Cooker, M.J., 2009. Flow patterns, sedimentation and deposit architecture under a hydraulic jump on a non-eroding bed: defining hydraulic-jump unit bars. Sedimentology 56, 1346-1367.

Macdonald, H.A., Wynn, R.B., Huvenne, V.A., Peakall, J., Masson, D.G., Weaver, P.P., McPhail, S.D., 2011a. New insights into the morphology, fill, and remarkable longevity (>0.2 m.y.) of modern deep-water erosional scours along the northeast Atlantic margin. Geosphere 7, 845-867.

Macdonald, H.A., Peakall, J., Wignall, P.B., Best, J., 2011b. Sedimentation in deep-sea lobe-elements: Implications for the origin of thickening-upward sequences. Journal of the Geological Society of London 168, 319-331.

Maier, K.L., Fildani, A., Paull, C.K., Graham, S.A., McHargue, T.R., Caress, D.W., McGann, M., 2011. The elusive character of discontinuous deep-water channels: New insights from Lucia Chica channel system, offshore California. Geology 39, 327-330.

Morris, S.A., Kenyon, N.H., Limonov, A.F., Alexander, J., 1998. Downstream changes of large-scale bedforms in turbidites around the Valencia channel mouth, north-west Mediterranean implications for palaeoflow reconstruction. Sedimentology 45, 365-377.

Morris, W.R., Normark, W.R., 2000. Sedimentologic and geometric criteria for comparing modern and ancient sandy turbidite elements. In: Weimer, P., Slatt, R.M., Coleman, J., Rosen, N.C., Nelson, H., Bouma, A.H., Styzen, M.J., Lawrence, D.T. (Eds.), Deep Water Reservoirs of the World. GCSSEPM Foundation, Houston, pp. 606-628.

Morris, W.R., Scheihing, M.H., Wickens, H.DeV., Bouma, A.H., 2000. Reservoir architecture of deepwater sandstones: examples from the Skoorsteenberg Formation, Tanqua Karoo Sub-basin, South Africa. In: Weimer, P., Slatt, R.M., Coleman, J., Rosen, N.C., Nelson, H., Bouma, A.H., Styzen, M.J., Lawrence, D.T. (Eds.), Deep Water Reservoirs of the World. GCSSEPM Foundation, Houston, pp. 629-666.

Morris, E.A., Hodgson, D.M., Brunt, R.L., Flint, S.S., 2014. Origin, evolution and anatomy of silt-prone submarine external levees. Sedimentology 61, 1734-1763.

Moscardelli, L., Wood, L., Mann. P., 2006. Mass-transport complexes and associated processes in the offshore area of Trinidad and Venezuela. American Association of Petroleum Geology Bulletin 90, 1059-1088.

Mutti, E., Normark, W.R., 1987. Comparing examples of modern and ancient turbidite systems: problems and concepts. In: Leggett, J.K., Zuffa, G.G. (Eds.), Marine Clastic Sedimentology: Concepts and Case Studies). Graham & Trotman, Oxford, pp. 1-38.

Mutti, E., Normark, W.R., 1991. An integrated approach to the study of turbidite systems. In: Weimer, P., Link, M.H. (Eds.), Seismic Facies and Sedimentary Processes of Submarine Fans and Turbidite Systems. Springer, New York, pp. 75-106.

Normark, W.R., Paull, C.K., Caress, D.W., Ussler, W., Sliter, R., 2009. Fine-scale relief related to late Holocene channel shifting within the

floor of the upper Redondo Fan, offshore Southern California. Sedimentology 56, 1690-1704.

Oliveira, C.M., Hodgson, D.M., Flint, S.S., 2009. Aseismic controls on in situ soft-sediment deformation processes and products in submarine slope deposits of the Karoo Basin, South Africa. Sedimentology 56, 1201-1225

Ortiz-Karpf, A., Hodgson, D.M., McCaffrey, W.D., 2015. The role of mass-transport complexes in controlling channel avulsion and the subsequent sediment dispersal patterns on an active margin: The Magdalena Fan, offshore Colombia. Marine and Petroleum Geology 64, 58-75.

Palanques, A., Kenyon, N.H., Alonso, B. Limonov, A., 1995. Erosional and depositional patterns in the Valencia mouth: An example of a modern channel-lobe transition zone channel. Marine Geophysical Researches 17, 503-517.

Parker, G., 1982. Conditions for the ignition of catastrophically erosive turbidity currents. Marine Geology 46, 307-327.

Parsons, D.R., Peakall, J., Aksu, A.E., Flood, R.D., Hiscott, R. N., Beşiktepe, Ş., Mouland, D., 2010. Gravity-driven flow in a submarine channel bend: direct field evidence of helical flow reversal. Geology 38, 1063-1066.

Paull, C.K., McGann, M., Sumner, E.J., Barnes, P.M., Lundsten, E.M., Anderson, K., Gwiazda, R., Edwards, B., Caress, D.W., 2014. Sub-

1149 decadal turbidite frequency during the early Holocene: Eel Fan,
1150 offshore northern California. Geology 42, 885-858.

1151 Peakall, J., Kane, I.A., Masson, D.G., Keevil, G., McCaffrey, W.,
1152 Corney, R., 2012. Global (latitudinal) variation in submarine channel
1153 sinuosity. Geology 40, 11-14.

1154 Peakall, J., Wells, M.G., Cossu, R., Kane, I. A., Masson, D. G., Keevil,
1155 G.M., McCaffrey, W., Corney, R., 2013. Global (latitudinal) variation
1156 in submarine channel sinuosity: reply. Geology 41, e288.

1157 Pickering, K.T., Hilton, V.C., 1998. Turbidite systems of southeast
1158 France, Vallis Press, London, 229 pp.

1159 Prélat, A., Hodgson, D.M., Flint, S.S., 2009. Evolution, architecture
1160 and hierarchy of distributary deep-water deposits: a high-resolution
1161 outcrop investigation from the Permian Karoo Basin, South Africa.
1162 Sedimentology 56, 2132-2154.

1163 Prélat, A., Hodgson, D.M., 2013. The full range of turbidite bed
1164 thickness patterns in submarine lobes: controls and implications.
1165 Journal of the Geological Society of London 170, 209-214.

1166 Pringle, J., Brunt, R.L., Hodgson, D.M., Flint, S.S., 2010. Capturing
1167 stratigraphic and sedimentological complexity from submarine
1168 channel complex outcrops to digital 3D models, Karoo Basin, South
1169 Africa. Petroleum Geoscience 16, 307-330.

1170 Pyles, D.R., Tomasso, M., Jennette, D.C., 2012. Flow processes and
1171 sedimentation associated with erosion and filling of sinuous
1172 submarine channels. Geology 40, 143-146.

1173 Sawyer, D.E., Flemings, P.B., Dugan, B., Germaine, J.T., 2009.
1174 Retrogressive failures recorded in mass transport deposits in the
1175 Ursa Basin, Northern Gulf of Mexico. Journal of Geophysical
1176 Research: Solid Earth 114, 1978-2012.

1177 Shaw, J., Puig, P., Han, G. 2013. Megaflutes in a continental shelf
1178 setting, Placentia Bay, Newfoundland. Geomorphology 189, 12-25.

1179 Sixsmith, P., Flint, S.S., Wickens, H. D., Johnson, S., 2004. Anatomy
1180 and stratigraphic development of a basin floor turbidite system in
1181 the Laingsburg Formation, main Karoo Basin, South Africa. Journal of
1182 Sedimentary Research 74, 239-254.

1183 Stevenson, C., Jackson, C.A-L., Hodgson, D.M., Hubbard, S.,
1184 Eggenhuisen, J., 2015. Deep-water sediment bypass. Journal of
1185 Sedimentary Research. DOI: 10.2110/jsr.2015.63

1186 Stow, D.A., Johansson, M., 2000. Deep-water massive sands: nature,
1187 origin and hydrocarbon implications. Marine and Petroleum Geology
1188 17, 145-174.

1189 Sullivan, M.D., Foreman, J.L., Jennette, D.C., Stern, D., Jensen, G.N.,
1190 Goulding, F.J., 2004. An integrated approach to characterization and
1191 modeling of deep-water reservoirs, Diana field, western Gulf of
1192 Mexico. In: Grammer, G.M., Harris, P.M., Eberli, G.P. (Eds.),

1193 Integration of outcrop and modern analogs in reservoir modelling.
1194 AAPG Memoir 80, pp. 215-234.

1195 Sumner, E.J., Amy, L.A., Talling, P.J., 2008. Deposit structure and
1196 processes of sand deposition from decelerating sediment
1197 suspensions. Journal of Sedimentary Research 78, 529-547.

1198 Sumner, E.J., Talling, P.J., Amy, L.A., Wynn, R.B., Stevenson, C.J.,
1199 Frenz, M., 2012. Facies architecture of individual basin-plain
1200 turbidites: Comparison with existing models and implications for
1201 flow processes. Sedimentology 59, 1850-1887.

1202 Sumner, E.J., Peakall, J., Parsons, D., Wynn, R., Darby, S., Dorrell, R.,
1203 McPhail, S., Perrett, J., Webb, A., White, D., 2013. First direct
1204 measurements of hydraulic jumps in an active submarine density
1205 current. Geophysical Research Letters 40, 5904-5908.

1206 Sumner, E.J., Peakall, J., Dorrell, R.M., Parsons, D.R., Darby, S.E.,
1207 Wynn, R.B., McPhail, S.D., Perrett, J., Webb, A., White, D., 2014.
1208 Driven around the bend: Spatial evolution and controls on the
1209 orientation of helical bend flow in a natural submarine gravity
1210 current. Journal of Geophysical Research: Oceans 119, 898-913.

1211 Talling, P.J., Masson, D.G., Sumner, E.J., Malgesini, G., 2012.
1212 Subaqueous sediment density flows: Depositional processes and
1213 deposit types. Sedimentology 59, 1937-2003.

1214 Tankard, A., Welsink, H., Aukes, P., Newton, R., Stettler, E., 2009.
1215 Tectonic evolution of the Cape and Karoo basins of South Africa.
1216 Marine and Petroleum Geology 26, 1379-1412.

Terlaky, V., Rocheleau, J., Arnott, R.W.C., 2015 Stratal composition and stratigraphic organization of stratal elements in an ancient deep-marine basin-floor succession, Neoproterozoic Windermere Supergroup, British Columbia, Canada Sedimentology. DOI:10.1111/sed.12222

van der Merwe, W.C., Hodgson, D.M., Brunt, R.L., Flint, S.S., 2014. Depositional architecture of sand-attached and sand-detached channel-lobe transition zones on an exhumed stepped slope mapped over a 2500 km^2 area. Geosphere 10, 1076-1093.

Van Der Werff, W., Johnson, S. 2003. High resolution stratigraphic analysis of a turbidite system, Tanqua Karoo Basin, South Africa. Marine and Petroleum Geology 20, 45-69.

Veevers, J., Cole, D., Cowan, E. 1994. Southern Africa: Karoo basin and Cape fold belt. In: Veevers, J.J., Powell, C.Mc.A. (Eds.), Permian-Triassic Pangean basins along the Panthalassan margin of Gondwanaland. Geological Society of America Memoir 184, pp. 223-279.

Vicente-Bravo, J.V., Robles, S., 1995. Large-scale mesotopographic bedforms from the Albian Black Flysch, northern Spain: characterization, setting and comparison with recent analogues. In: Pickering, K.T., Hiscott, R.N., Kenyon, N.H., Ricci-Lucchi, F., Smith, R.D.A. (Eds), Atlas of Deep Water Environments; Architectural Style in Turbidite Systems. Chapman & Hall, London, pp. 282-286.

1240 Visser, J.N.J., 1993. Sea-level changes in a back-arc-foreland
1241 transition: the late Carboniferous-Permian Karoo Basin of South
1242 Africa. Sedimentary Geology 83, 115-131.

1243 Wei, T., Peakall, J., Parsons, D.R., Chen, Z., Zhao, B., Best, J., 2013.
1244 Three-dimensional gravity-current flow within a subaqueous bend:
1245 Spatial evolution and force balance variations. Sedimentology 60,
1246 1668-1680.

1247 Wickens H.DeV., 1994. Basin floor fan building turbidites of the
1248 southwestern Karoo Basin, Permian Ecca Group, South Africa. PhD-
1249 Thesis, University of Port Elizabeth.

1250 Wickens, H.DeV., Bouma, A.H., 2000. The Tanqua fan complex,
1251 Karoo Basin, South Africa-outcrop analog for fine-grained,
1252 deepwater deposits. In: Bouma, A.H., Stone, C.G. (Eds.), Fine-grained
1253 Turbidite Systems. AAPG Memoir 72, pp. 153-164.

1254 Winn, R.D., Dott, R.H., 1979. Deep-water fan-channel conglomerates
1255 of Late Cretaceous age, southern Chile. Sedimentology 26, 203-228.

1256 Wynn, R.B., Kenyon, N.H., Masson, D.G., Stow, D.A., Weaver, P.P.,
1257 2002a. Characterization and recognition of deep-water channel-lobe
1258 transition zones. AAPG Bulletin 86, 1441-1462.

1259 Wynn, R.B., Piper, D.J.W., Gee, M.J.R., 2002b. Generation and
1260 migration of coarse-grained sediment waves in turbidity current
1261 channels and channel-lobe transition zones. Marine Geology 192,
1262 59-78.

Young, R.A., Slatt, R.M., Staggs, J.G., 2003. Application of ground penetrating radar imaging to deepwater (turbidite) outcrops. Marine and Petroleum Geology 20, 809-821.

Figure captions

Fig. 1. Location map of the Laingsburg and Tanqua depocentres within the Western Cape (South Africa) and schematic interpretations of the Fan 3 and Unit A5 fan systems (based on Sixsmith et al. (2004) and Hodgson et al. (2006)). Imaged from Google Earth.

Fig. 2. Stratigraphic column of the deep-water deposits from the Laingsburg depocentre and the Tanqua depocentre, based on Prélat et al. (2009) and Flint et al. (2011). The fan systems discussed in this paper (Fan 3 and Unit A5) are highlighted.

Fig. 3. Detailed maps of case study areas with locations of sedimentary logs, and outlines of Fan3 (A) and Unit A5 (B). Solid line in A indicates the main profile illustrated in Fig. 6, while the dotted lines indicate the additional profiles of Fig. 10A. Image from Google Earth.

Fig. 4. Main sedimentary facies in the case study areas, with (A) structureless fine-grained sandstone with floating siltstone clast (Fa1) – Unit A5; (B) Steepening of angle of climb within climbing ripple-laminated sandstone bed tostoss-side preserved climbing ripples (Fa2)– Fan 3; (C) Banded sandstone (Fa3) – Unit A5; (D)

Lateral discontinuous thin-bedded siltstones and sandstones with small-scale erosive marks – UnitA5 (Fa4-2).

Fig. 5. (A) Representative facies photographs from the Fan 3 feature. (A1) Thin-bedded sandstone and siltstone deposits showing the difference in character below (Fa4-1) and above (Fa4-2) the basal erosion surface. (A2) Internal truncation within medium-bedded banded sandstone. (A3) Truncation surface on top of thin-bedded fine-grained deposits with structured (rippled) sandstone on top and mudstone clast conglomerate at the base. (A4) Undulating basal erosion surface truncating thin-bedded deposits. (A5) Photopanel of the steep stepped southern margin with the locations of A1 and A2 indicated. (B) Representative facies photographs of Unit A5 feature indicated in Fig.11C with (B1) Thin-bedded siltstones interbedded with occasional thin coarse-grained sandstone (indicated by white arrows). Individual siltstone beds show thicknesses >3cm (Fa4-2). (B2) Small scale soft-sediment deformed sandstones (Fa6). Folds are indicated y white lines. (B3) Composite erosion surface with initial mudstone clast conglomerate and banded sandstones, with laminae parallel to the erosion surface, on top. (B4) Pinchout of sandstone bed within siltstone thin-beds of the western margin indicated by the white line.

Fig. 6. Facies correlation panel of main section (solid line in Fig. 3A) of the erosional feature at Kleine Riet Fontein in Fan 3 with palaeocurrents shown, with n = number of measurements, μ = mean palaeoflow and σ = standard deviation. Solid white lines indicate bed

boundaries. The fill is divided into a lower (LP) and upper package (UP) and a total of seven infill elements as indicated in the bottom right cartoon. The boundary between the lower and upper package is indicated by a light blue dashed line. Facies association 1 (Fa1) has been subdivided into structureless and banded and/or planar laminated facies; Facies association 2 (Fa2) has been subdivided into ripple and planar laminated facies.

Fig. 7. Palaeocurrent distribution within the Kleine Riet Fontein area (Fan 3) subdivided into underlying, fill and overlying deposits.. The asterisk shows the more detailed stratigraphic change in palaeoflow direction as also indicated in the main correlation panel of Fig. 6 (K7).

Fig. 8. (A) Fence diagram showing the 3D architecture of the Kleine Riet Fontein (Fan3) erosional feature. Palaeoflow of the underlying thin-bedded deposits is indicated (336°). The infill thins-out both in the eastward and southward directions. See Fig. 3A for log locations. (B) Detailed log of the fill (K8) showing the division in infill elements (IE). IE 3 is pinching-out at K8, but is possibly represented by a thin by-pass interval separating IE2 and IE4.

Fig. 9. Panoramic view of infill element 3 (C), with (C1) Truncation of elements in southern direction, and (C2) Abrupt bed pinch-out in the northern direction. Solid white lines indicate bed boundaries, solid red line indicates the basal erosional surface, and the dashed red line an internal truncation surface.

Fig. 10. Panoramic photopanel and division in infill elements, displaying the internal architecture within the Kleine Riet Fontein erosional feature (Fan 3). The top figure shows seven discrete sedimentary packages defined as different infill elements. The boxes show the locations of Inset A & B and Inset C (Fig. 9). The internal architecture of these elements shows complicated bed architectures and stacking patterns with abrupt pinch-out of beds in both southwards and northwards directions. Element 4 (Inset A) and 5 (Inset B) both show stacked bedsets with depositional dips in an overall southern (updip) direction.

Fig. 11. (A) Panoramic view of the Unit A5 case study showing the undulating western (updip) margin. (B) Facies correlation panel of the Unit A5 feature and W15 sedimentary log of scour-fill showing a coarsening/thickening upward pattern within the infill and a fining/thinning upward trend on top of the fillThe overlying A5-A6 mud is used as the datum for the sedimentary logs, but is not included in this panel. (C) Zoomed-in section of the western margin. Locations of the Unit A5 facies photos within Fig. 5 are indicated. See Fig. 6 for additional explanatory information.

Fig. 12. Streamlines based on Allen (1971) and possible linkage to lateral and stratigraphic variance observed at K7, K8 and K9 with n = number of measurements, μ = mean palaeoflow and σ = standard deviation. These streamlines account for an idealised megaflute morphology with an orientation of 336° (based on underlying deposits). See Fig. 6 for log location and exact stratigraphic intervals.

Fig. 13. Depositional history interpretation of infill elements based on the main profile given in Fig. 6 of the Kleine Riet Fontein (Fan 3) erosional feature. It is unknown how far the deposits of element 1, 2 and 3 extended on the southern margin as the basal surface of element 5 has removed a substantial part of this. The palaeocurrent distribution of the underlying thin-beds is oriented to the NNW (336°). It must be noted that this section includes a significant change in orientation around log K6from 345° (almost parallel to the underlying palaeoflow) to 030° (transverse to the underlying palaeoflow), indicated within the map at the bottom right. Imaged from Google Earth.

Fig. 14. Cross plot of width and depth data of scours and megaflutes from ancient (outcrop) and modern systems. Scour data from Macdonald (2011a). Channel trendline is based on Clark and Pickering (1996).

Fig. 15. Simplified conceptual model to explain alternative ways of preservation of long-lived composite scours from the initial (T1) to final depositional setting (T2), divided by vertical infill patterns – Coarsening and thickening (A) or fining and thinning (B). Two scenarios are proposed for infill pattern A: A1 – Scour preservation adjacent to erosionally-confined channel progradation and successive increase in overbank deposition; A2 – Scour preservation at the maximum extent of channel progradation followed by lobe retrogradation. Two alternative scenarios are proposed for infill pattern B: B1 – Scour preservation adjacent to depositionally-

1386 confined channel progradation and successive development of the
1387 levee; B2 – Scour preservation due to channel avulsion and
1388 successive infill of scours by lobe fringe materials. The ‘*’ indicates
1389 initial position of the middle scour at T1.

1390

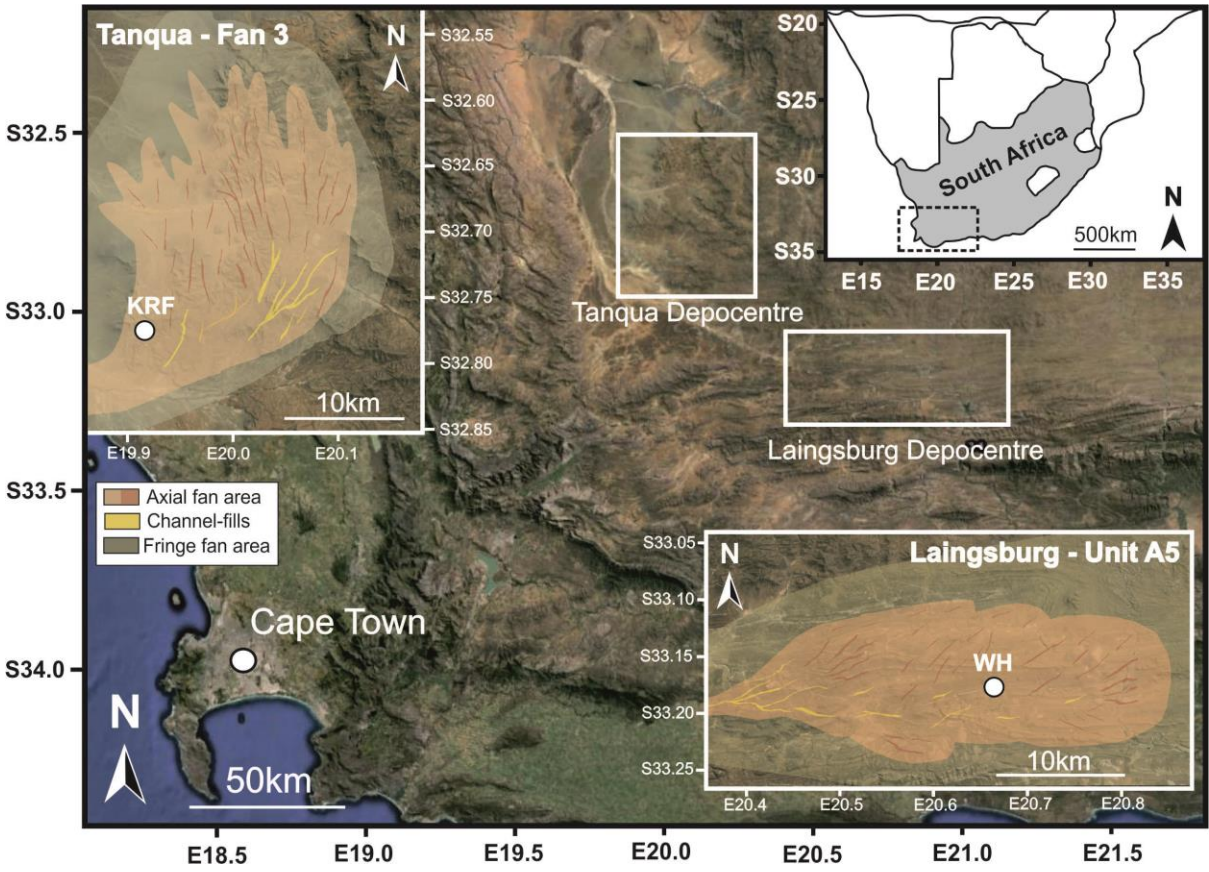
Tanqua - Fan 3
N
S32.55
S32.60
S32.65
S32.70
S32.75
S32.80
S32.85
KRF
10km
E19.9
E20.0
E20.1
S20
S25
S30
S35
South Africa
N
500km
E15
E20
E25
E30
E35
Tanqua Depocentre
Laingsburg Depocentre
Axial fan area
Channel-fills
Fringe fan area
S32.5
S33.0
S33.5
S34.0
Cape Town
N
50km
S33.05
S33.10
S33.15
S33.20
S33.25
N
Laingsburg - Unit A5
WH
10km
E20.4
E20.5
E20.6
E20.7
E20.8
E18.5
E19.0
E19.5
E20.0
E20.5
E21.0
E21.5

1391

1392

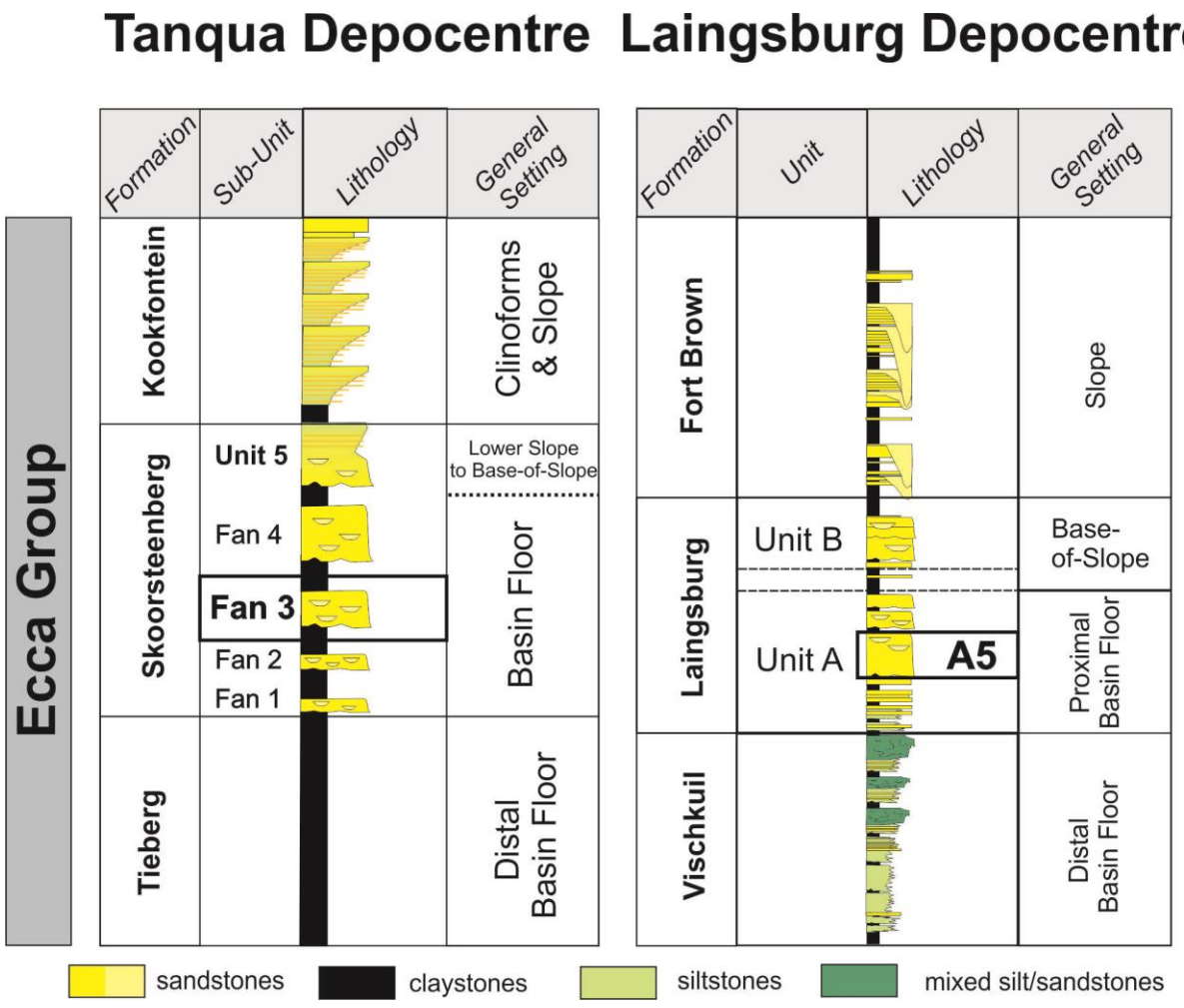
Tanqua Depocentre
Laingsburg Depocentre
Ecca Group
Formation
Sub-Unit
Lithology
General Setting
Kookfontein
Clinoforms & Slope
Skoorsteenberg
Unit 5
Fan 4
Fan 3
Fan 2
Fan 1
Lower Slope to Base-of-Slope
Basin Floor
Tieberg
Distal Basin Floor
Formation
Unit
Lithology
General Setting
Fort Brown
Slope
Laingsburg
Unit B
Unit A
A5
Base-of-Slope
Proximal Basin Floor
Vischkuil
Distal Basin Floor
sandstones
claystones
siltstones
mixed silt/sandstones

1393

1394

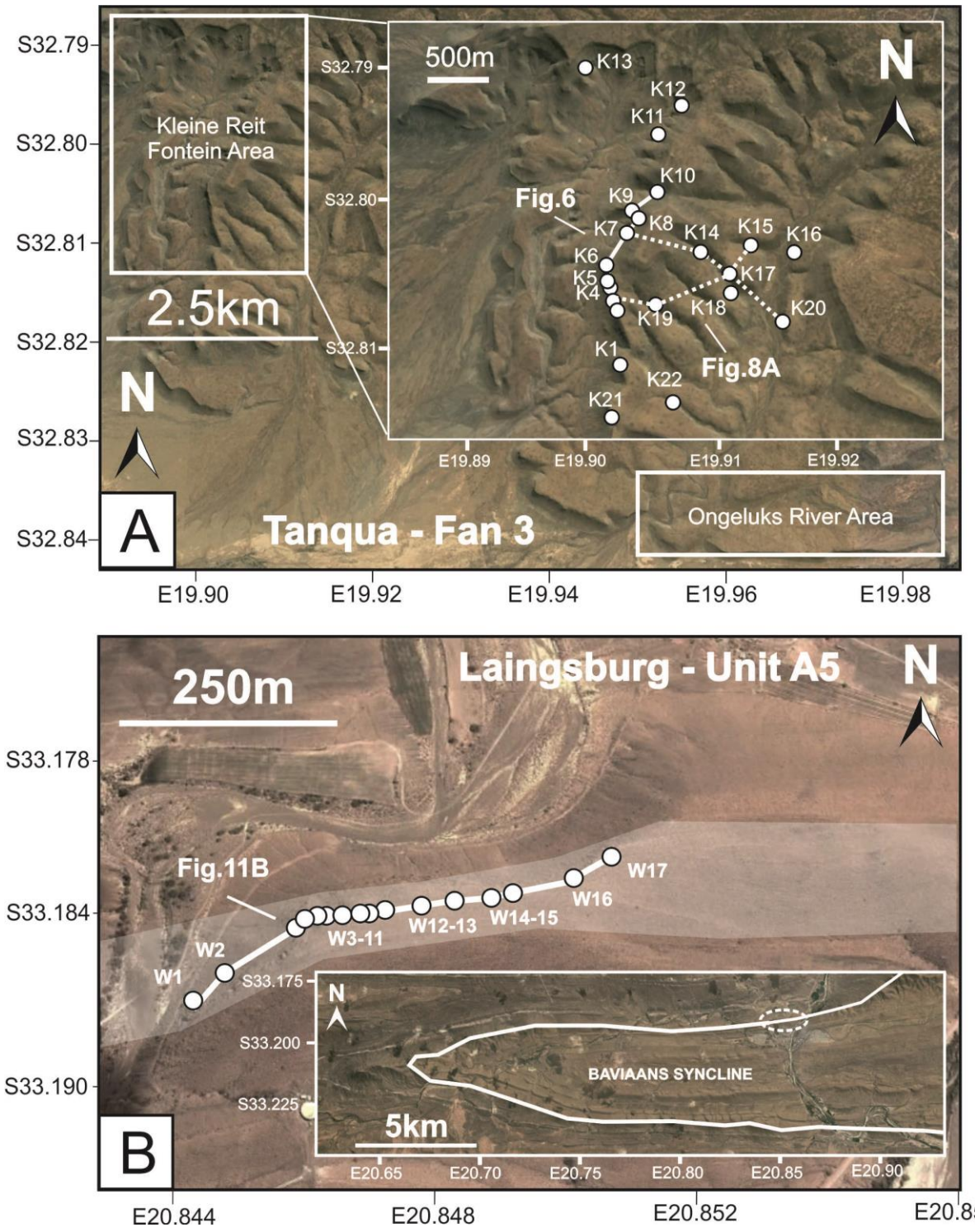
S32.79
S32.80
S32.81
S32.82
S32.83
S32.84
E19.90
E19.92
E19.94
E19.96
E19.98
Kleine Reit Fontein Area
2.5km
N
A
Tanqua - Fan 3
Ongeluks River Area
500m
K13
K12
K11
K10
K9
K8
K7
K6
K5
K4
K14
K15
K16
K17
K18
K19
K20
K1
K22
K21
Fig.6
Fig.8A
E19.89
E19.90
E19.91
E19.92
Laingsburg - Unit A5
250m
S33.178
S33.184
S33.190
E20.844
E20.848
E20.852
E20.856
Fig.11B
W1
W2
W3-11
W12-13
W14-15
W16
W17
S33.175
S33.200
S33.225
BAVIAANS SYNCLINE
5km
B
E20.65
E20.70
E20.75
E20.80
E20.85
E20.90

1395

1396

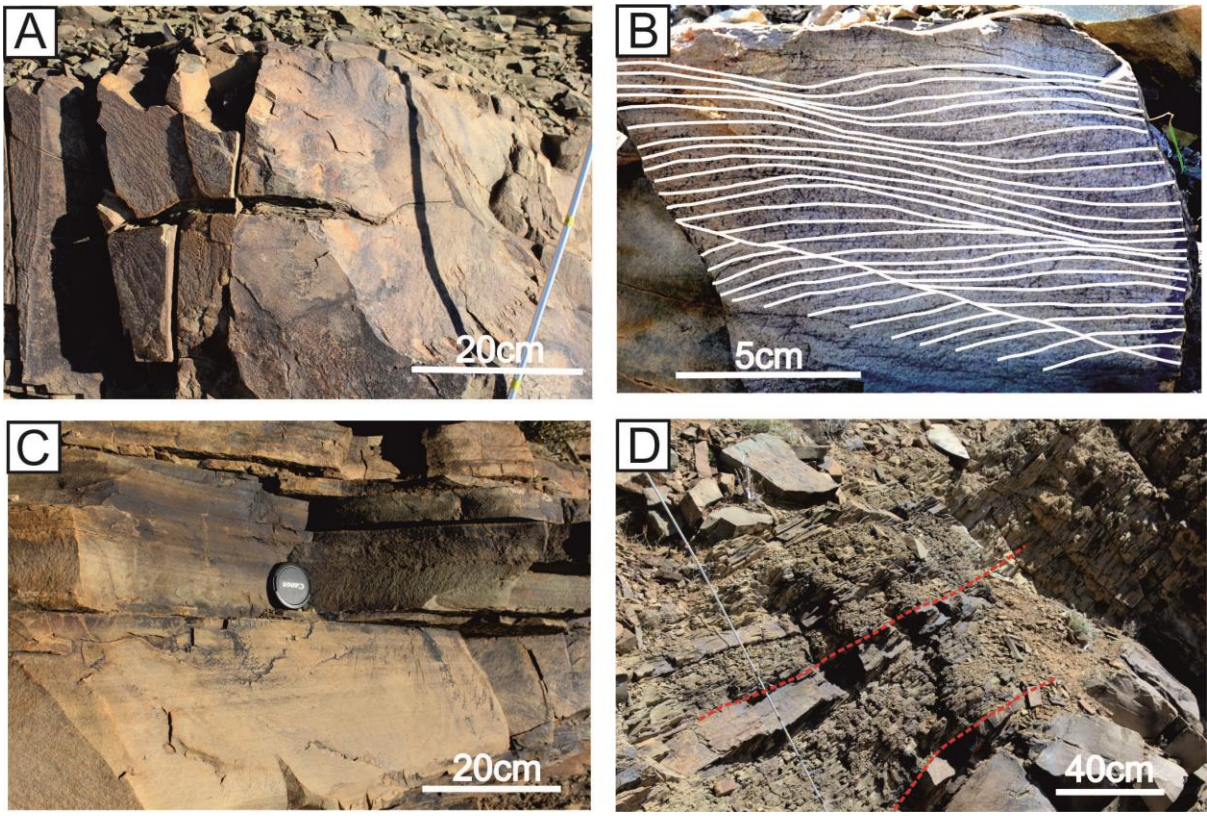

1397

1398

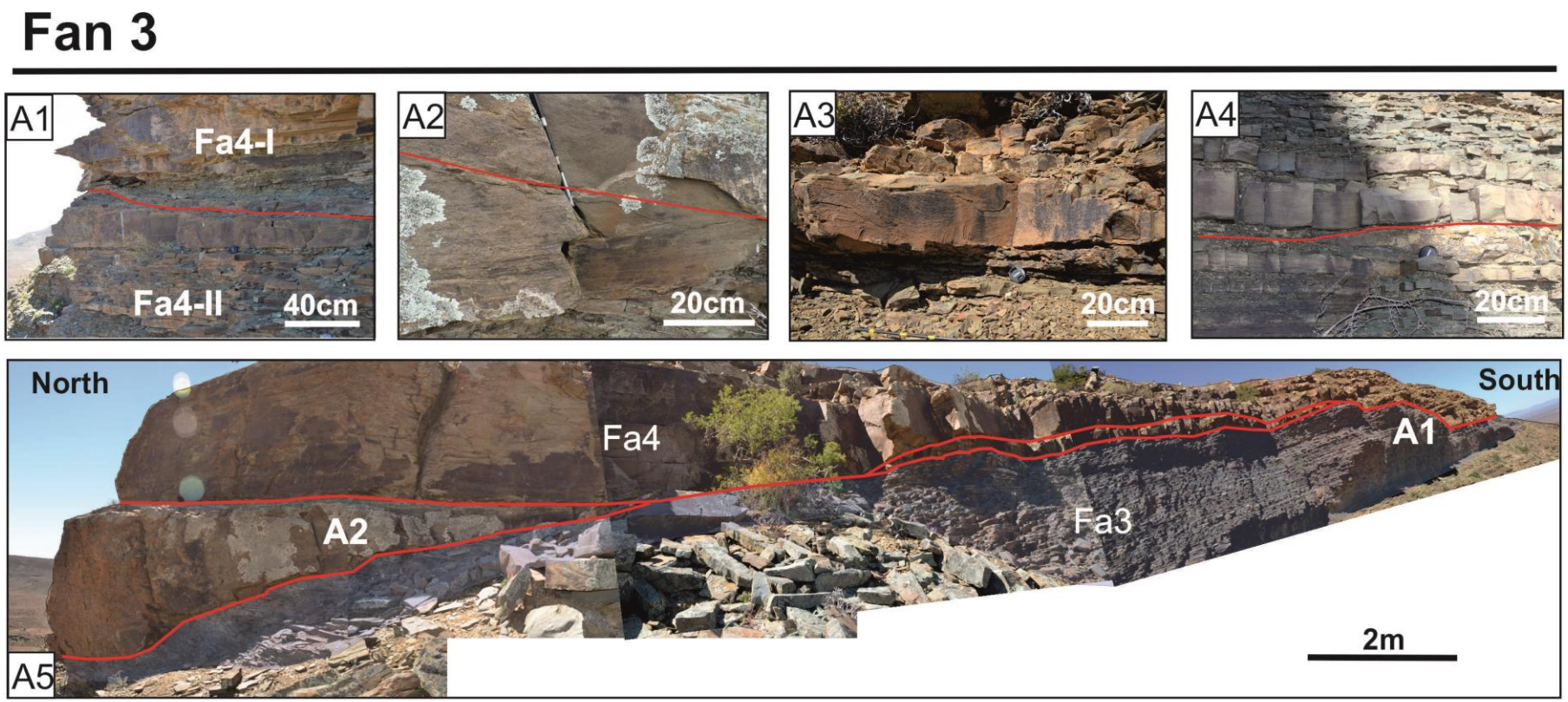
Fan 3
A1
Fa4-I
Fa4-II
40cm
A2
20cm
A3
20cm
A4
20cm
North
South
Fa4
A1
A2
Fa3
2m
A5
Unit A5
Erosional surface
B1
10cm
B2
10cm
B3
20cm
B4
20cm

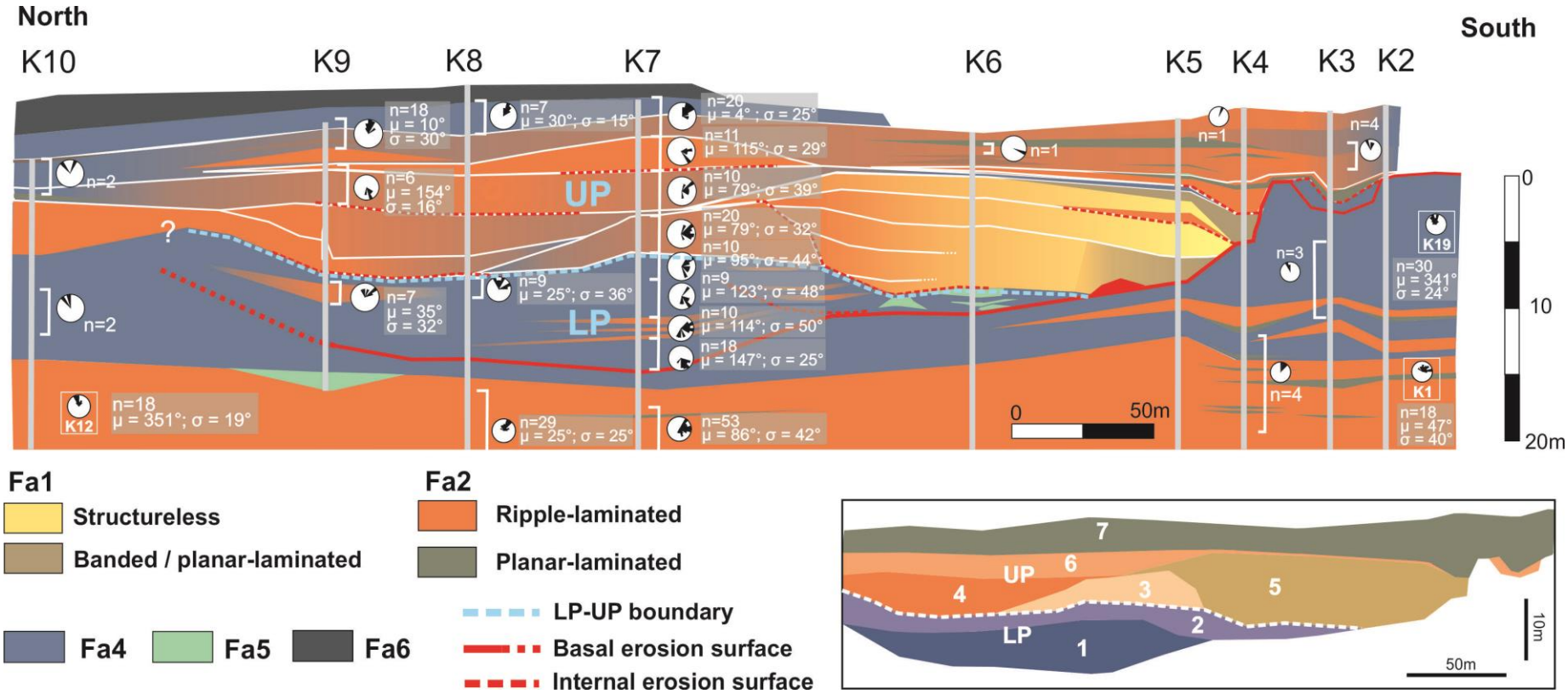

Fa1

- Structureless
- Banded / planar-laminated

Fa2

- Ripple-laminated
- Planar-laminated

- Fa4
- Fa5
- Fa6

- LP-UP boundary
- Basal erosion surface
- Internal erosion surface

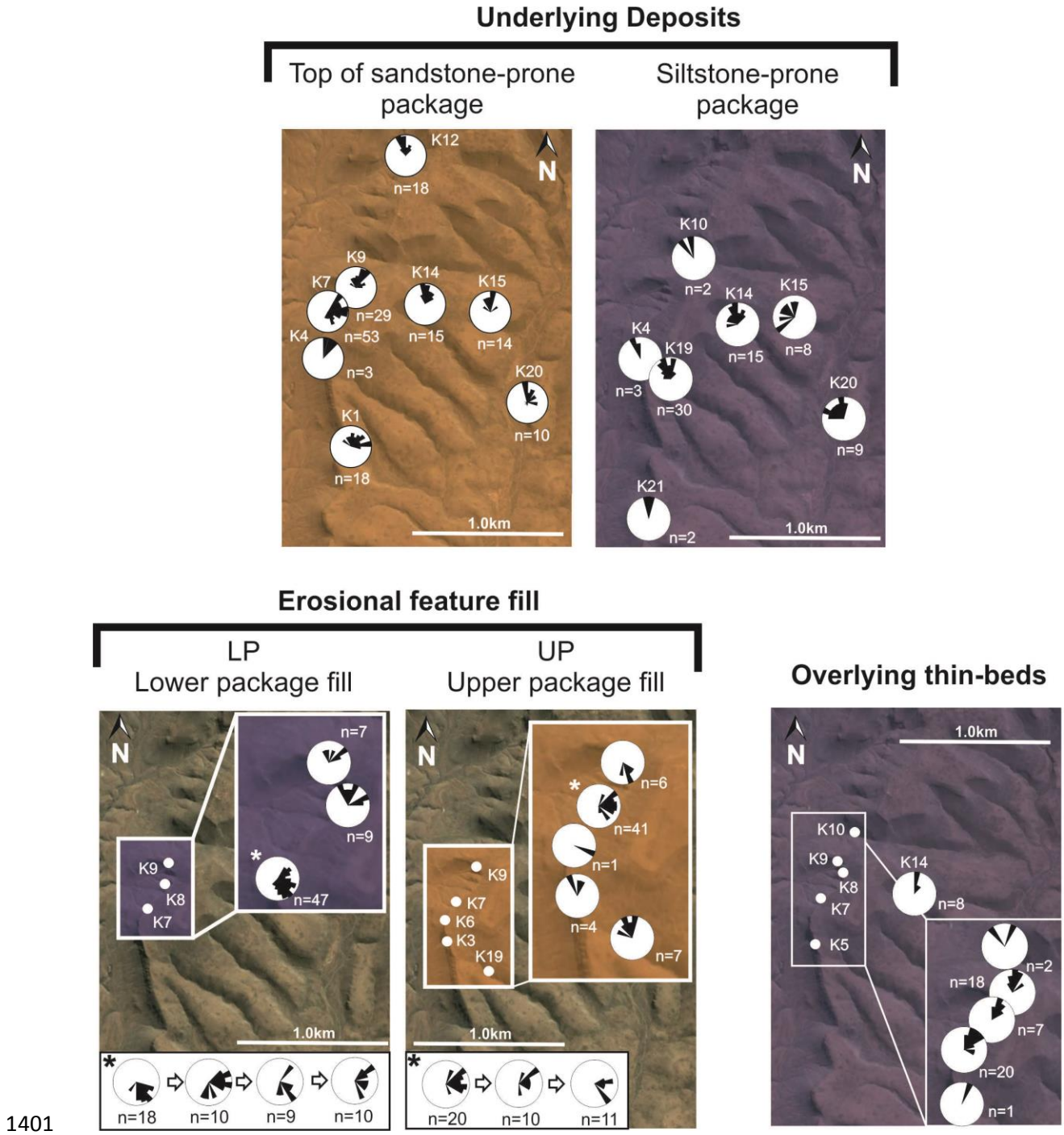
Underlying Deposits
Top of sandstone-prone package
Siltstone-prone package
K12
n=18
N
K9
K7
n=29
K14
K15
K4
n=53
n=15
n=14
n=3
K20
n=10
K1
n=18
1.0km
N
K10
n=2
K14
K15
K4
K19
n=15
n=8
n=3
n=30
K20
n=9
K21
n=2
1.0km
Erosional feature fill
LP
Lower package fill
UP
Upper package fill
Overlying thin-beds
N
n=7
n=9
K9
K8
K7
*
n=47
1.0km
*
n=18
n=10
n=9
n=10
N
n=6
*
n=41
n=1
K9
K7
K6
K3
K19
n=4
n=7
1.0km
*
n=20
n=10
n=11
N
1.0km
K10
K9
K8
K7
K5
K14
n=8
n=2
n=18
n=7
n=20
n=1

1401

1402

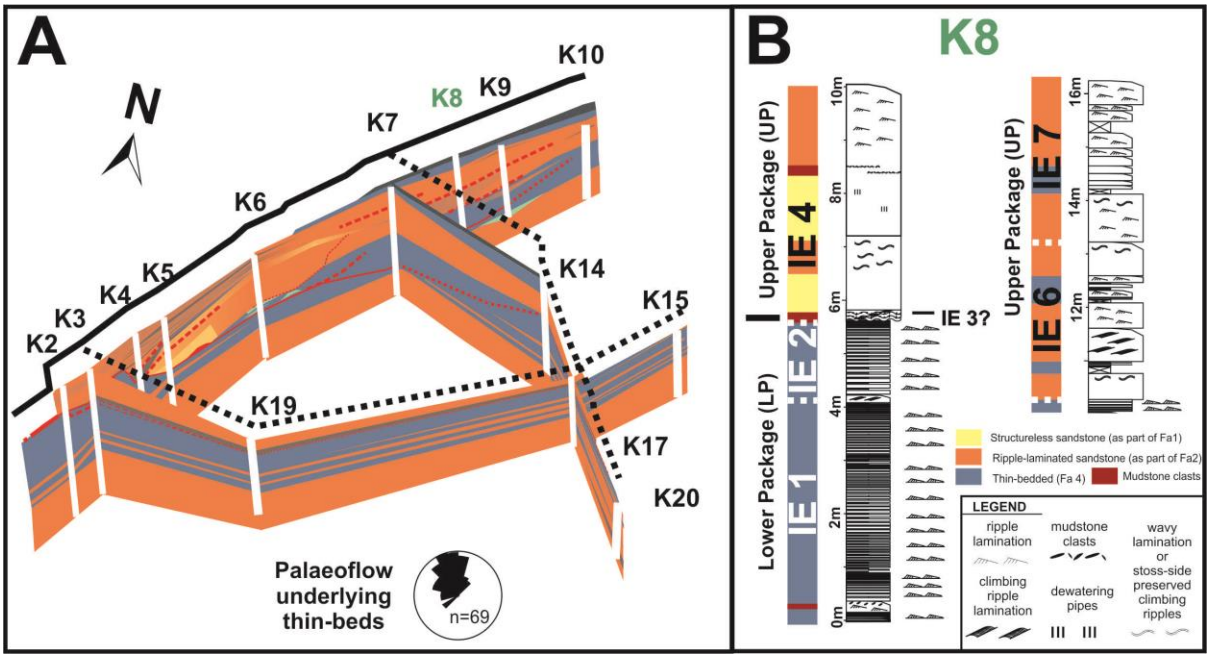
A
N
K10
K9
K8
K7
K6
K5
K4
K3
K2
K14
K15
K19
K17
K20
Palaeoflow
underlying
thin-beds
n=69
B
K8
Upper Package (UP)
IE 4
IE 2
IE 1
Lower Package (LP)
IE 3?
IE 7
IE 6
Upper Package (UP)
10m
8m
6m
4m
2m
0m
16m
14m
12m
Structureless sandstone (as part of Fa1)
Ripple-laminated sandstone (as part of Fa2)
Thin-bedded (Fa 4)
Mudstone clasts
LEGEND
ripple lamination
mudstone clasts
wavy lamination or stoss-side preserved climbing ripples
climbing ripple lamination
dewatering pipes

1403

1404

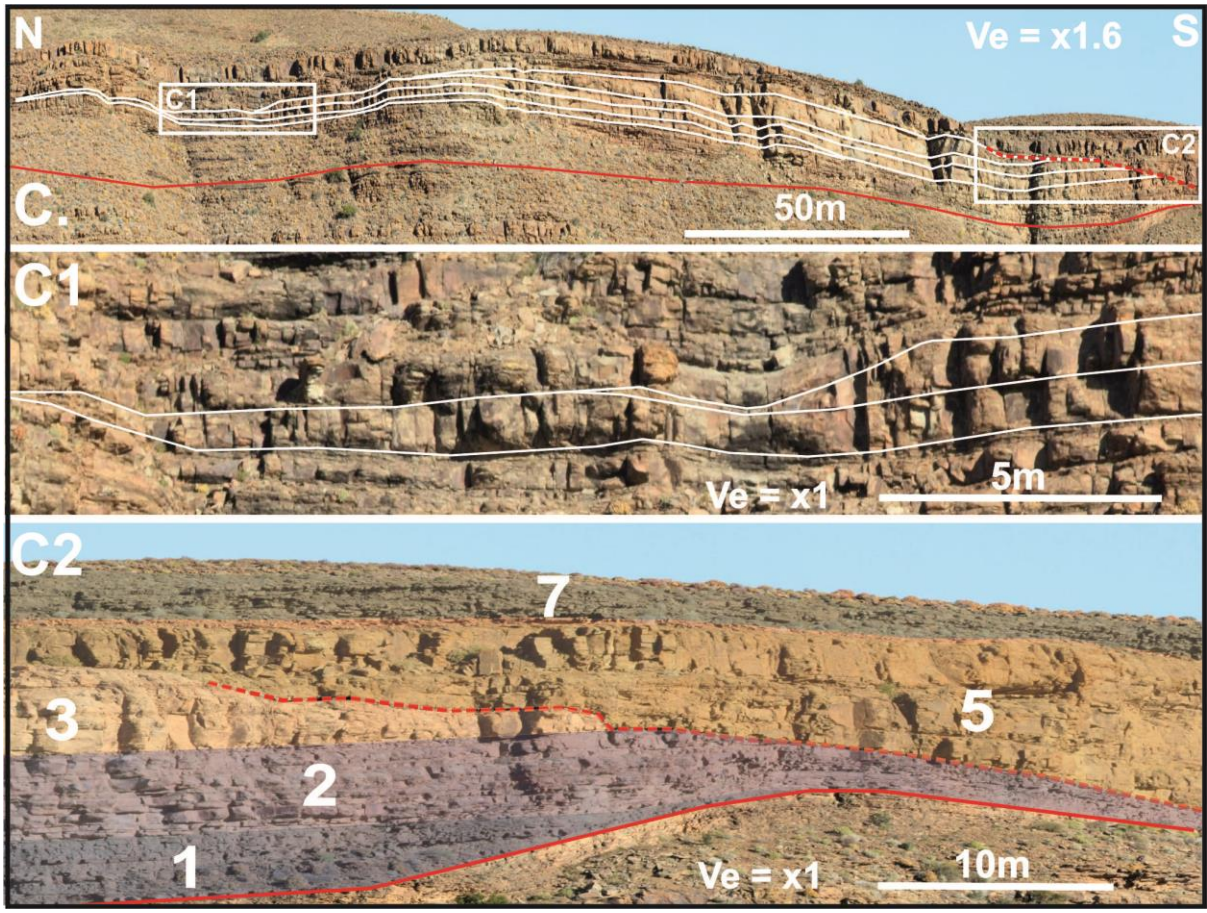

1405

1406

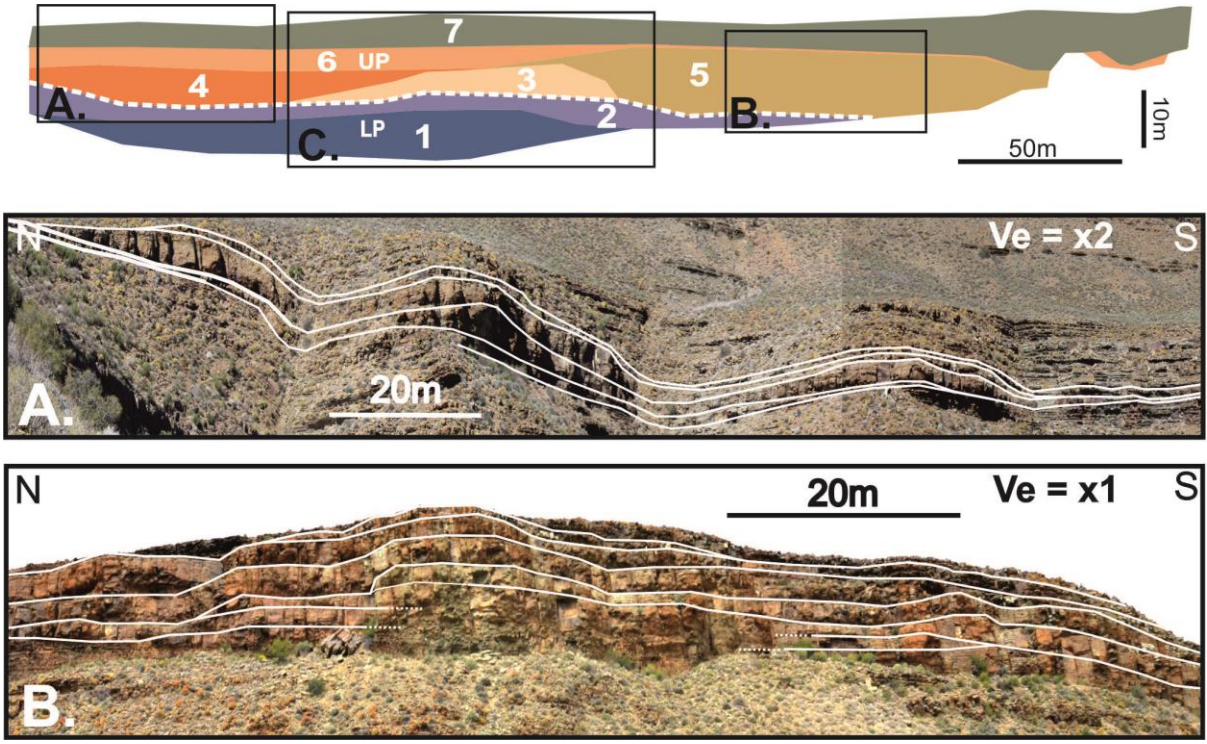

1407

1408

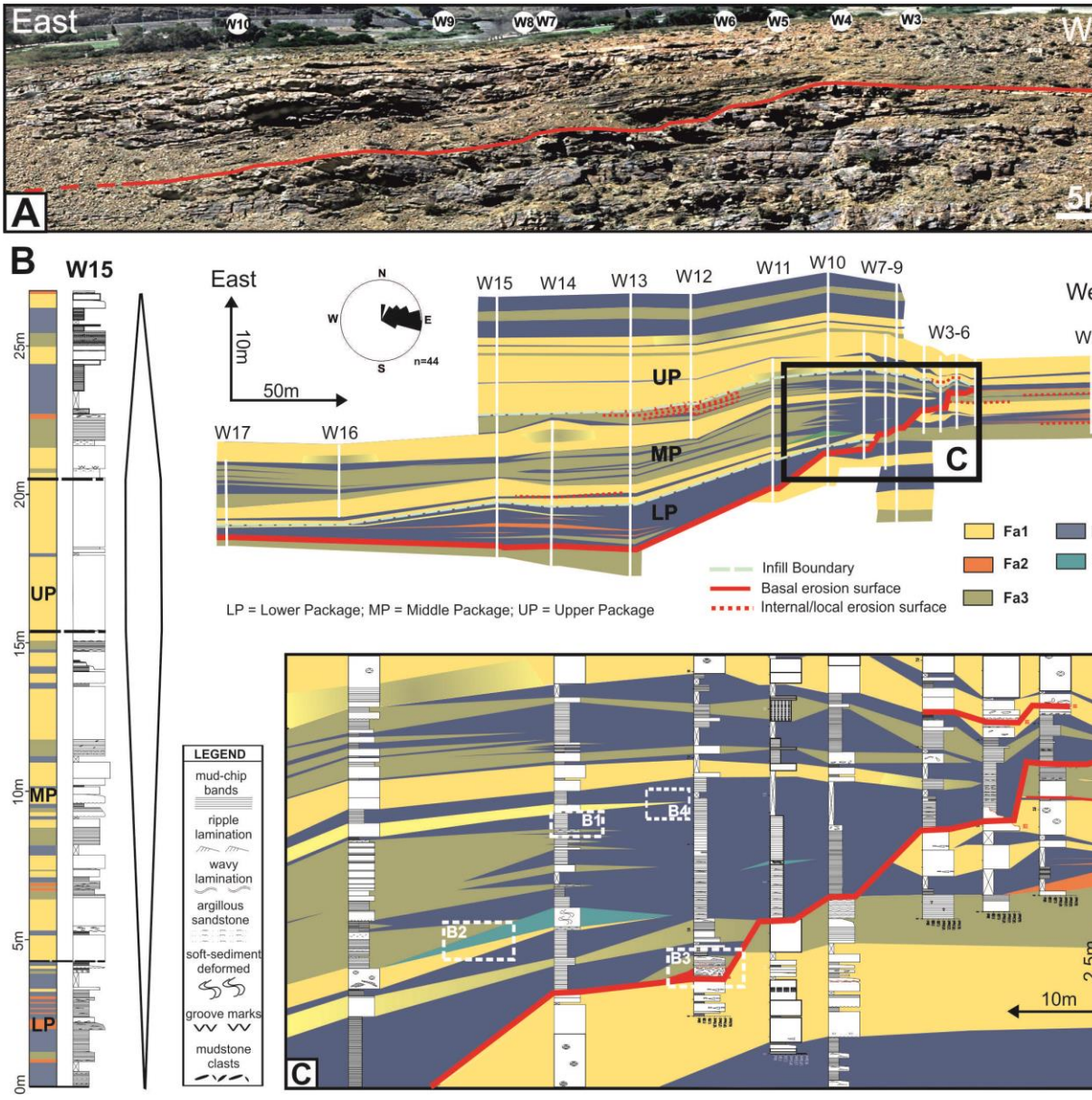
East
W10
W9
W8
W7
W6
W5
W4
W3
A
B
W15
25m
20m
15m
10m
5m
0m
UP
MP
LP
East
10m
50m
N
W
E
S
n=44
W15
W14
W13
W12
W11
W10
W7-9
W3-6
W17
W16
UP
MP
LP
C
Fa1
Fa2
Fa3
Infill Boundary
Basal erosion surface
Internal/local erosion surface
LP = Lower Package; MP = Middle Package; UP = Upper Package
LEGEND
mud-chip bands
ripple lamination
wavy lamination
argillous sandstone
soft-sediment deformed
groove marks
mudstone clasts
B1
B2
B3
B4
10m
C

1409

1410

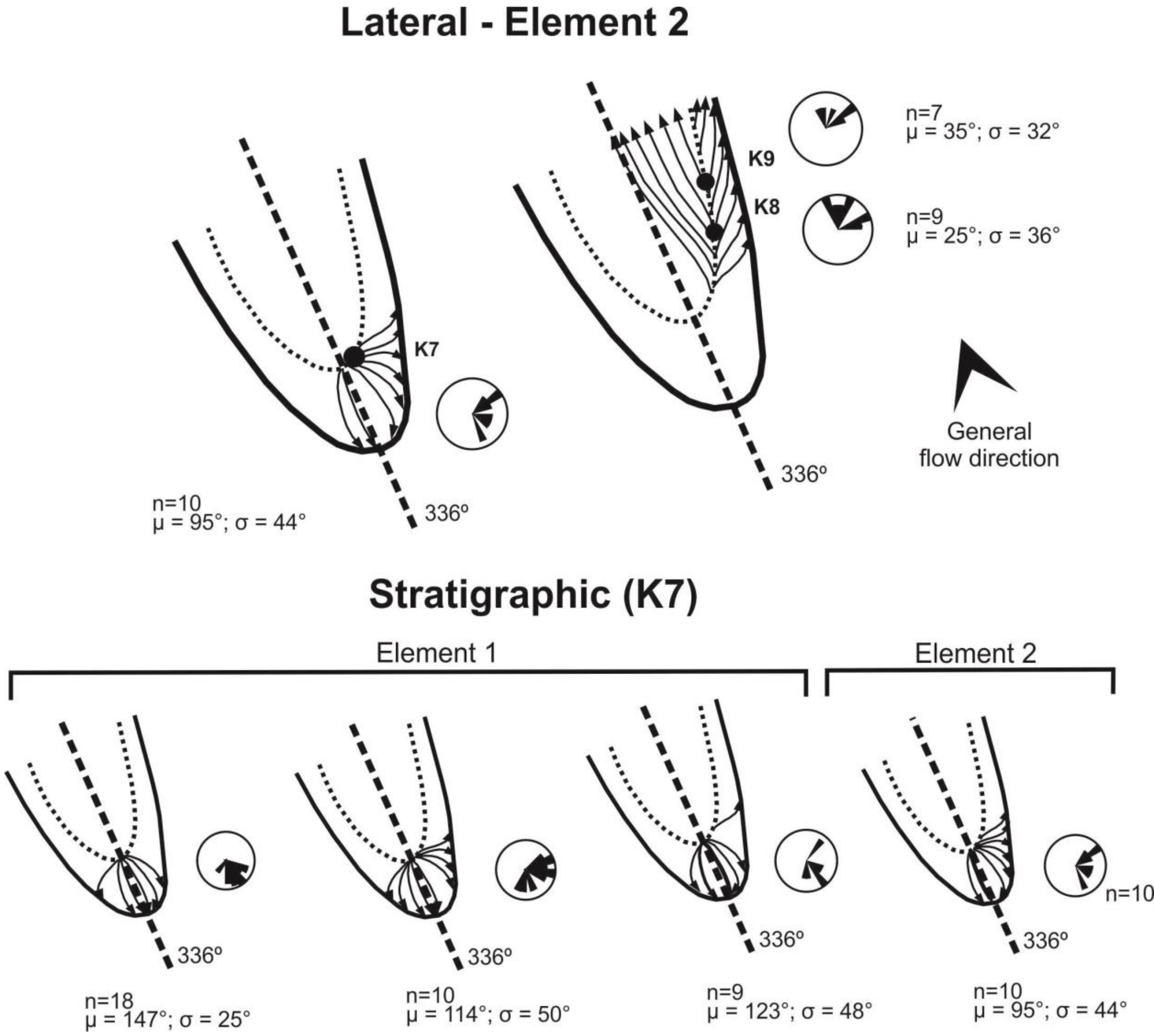
Lateral - Element 2
K7
n=10
μ = 95°; σ = 44°
336º
K9
K8
n=7
μ = 35°; σ = 32°
n=9
μ = 25°; σ = 36°
336º
General
flow direction
Stratigraphic (K7)
Element 1
Element 2
336º
336º
336º
336º
n=10
n=18
μ = 147°; σ = 25°
n=10
μ = 114°; σ = 50°
n=9
μ = 123°; σ = 48°
n=10
μ = 95°; σ = 44°

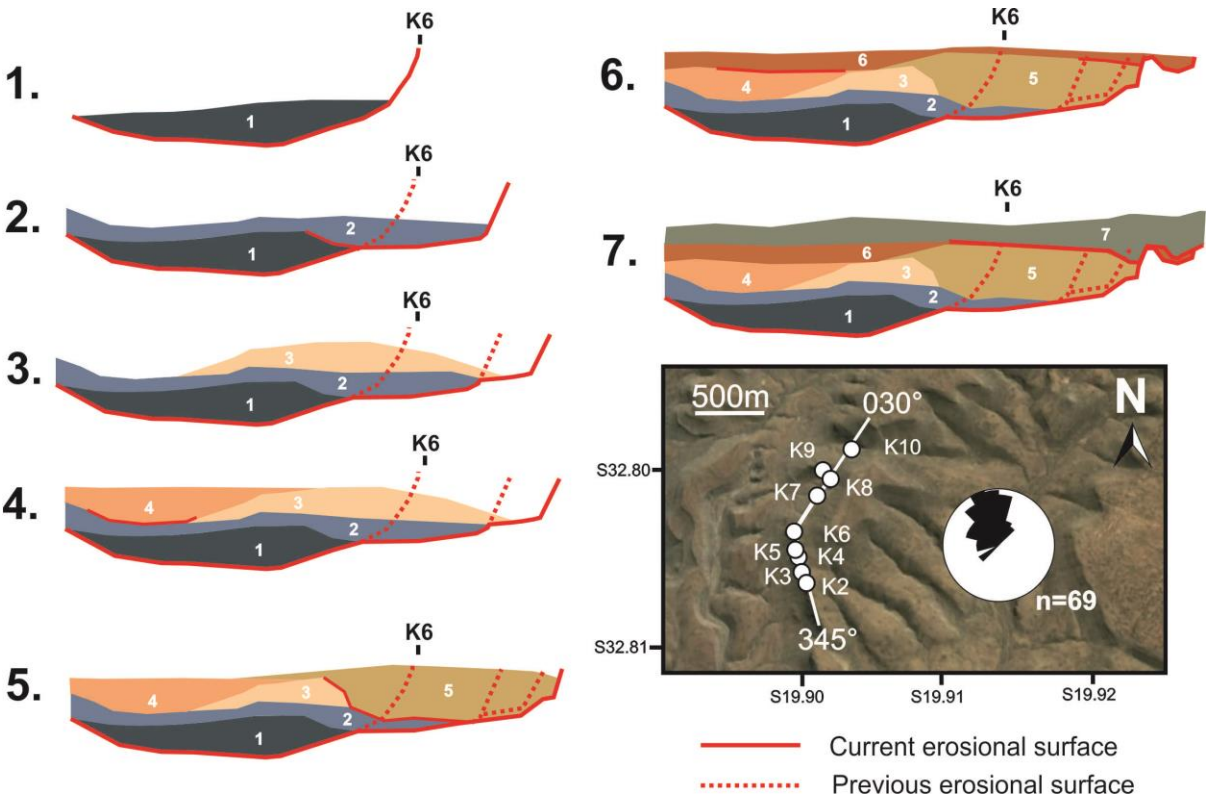
1.
K6
1
2.
K6
2
1
3.
K6
3
2
1
4.
K6
4
3
2
1
5.
K6
4
3
5
2
1
6.
K6
6
4
3
5
2
1
7.
K6
7
6
4
3
5
2
1
500m
030°
N
K9
K10
K7
K8
K6
K5
K4
K3
K2
345°
n=69
S32.80
S32.81
S19.90
S19.91
S19.92
Current erosional surface
Previous erosional surface

1413

1414

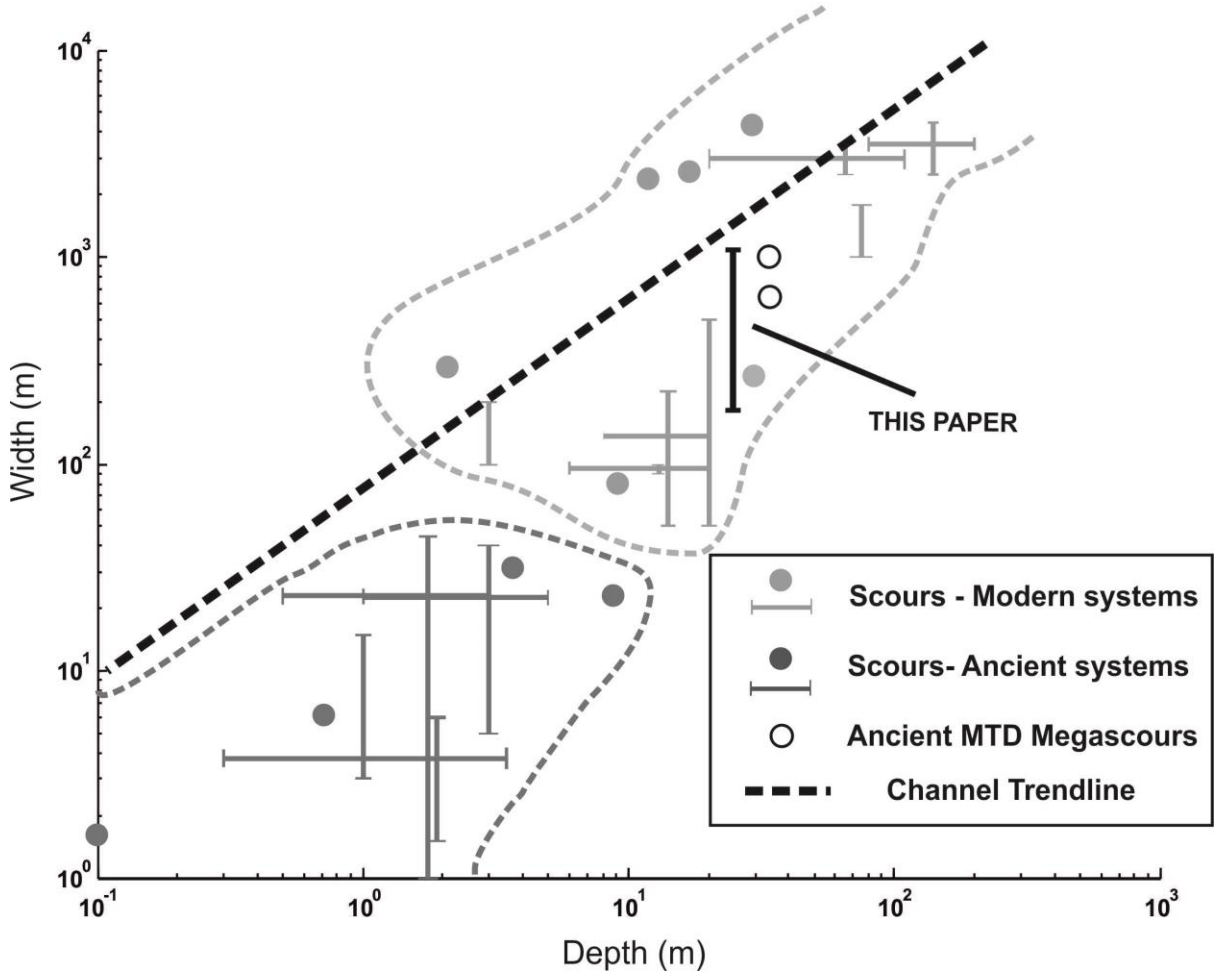
Width (m)
Depth (m)
THIS PAPER
Scours - Modern systems
Scours- Ancient systems
Ancient MTD Megascours
Channel Trendline

1415

1416

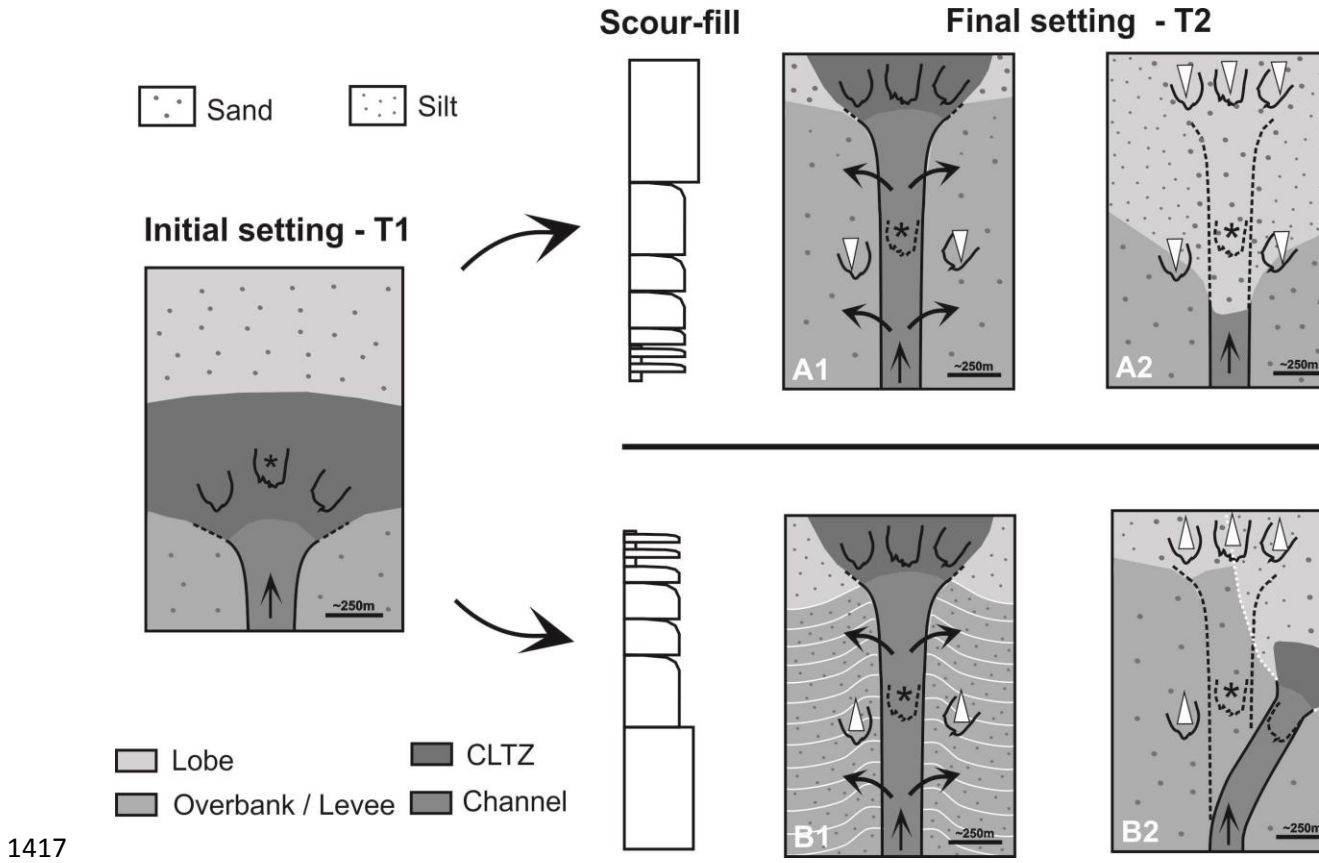
Scour-fill
Final setting - T2
Sand
Silt
Initial setting - T1
~250m
A1
A2
B1
B2
Lobe
CLTZ
Overbank / Levee
Channel

1417

1418